



Common origin of radiative neutrino mass, dark matter and leptogenesis in scotogenic Georgi-Machacek model

Shao-Long Chen ^{a,b,*}, Amit Dutta Banik ^{a,*}, Ze-Kun Liu ^{a,*}

^a Key Laboratory of Quark and Lepton Physics (MoE) and Institute of Particle Physics, Central China Normal University, Wuhan 430079, China

^b Center for High Energy Physics, Peking University, Beijing 100871, China

Received 3 January 2021; received in revised form 7 March 2021; accepted 2 April 2021

Available online 7 April 2021

Editor: Hong-Jian He

Abstract

We explore the phenomenology of the Georgi-Machacek model extended with two Higgs doublets and vector fermion doublets invariant under $SU(2)_L \times U(1)_Y \times \mathcal{Z}_4 \times \mathcal{Z}_2$. The \mathcal{Z}_4 symmetry is broken spontaneously while the imposed \mathcal{Z}_2 symmetry forbids triplet fields to generate any vacuum expectation value and leading to an inert dark sector providing a viable candidate for dark matter and generate neutrino mass radiatively. Another interesting feature of the model is leptogenesis arising from decay of vector-like fermions. A detailed study of the model is pursued in search for available parameter space consistent with the theoretical and experimental observations for dark matter, neutrino physics, flavor physics, matter-antimatter asymmetry in the Universe.

© 2021 Published by Elsevier B.V. This is an open access article under the CC BY license (<http://creativecommons.org/licenses/by/4.0/>). Funded by SCOAP³.

1. Introduction

Evidences from cosmology and astrophysics claim that about a quarter of the Universe is made up of dark matter [1]. However, the nature of dark matter remains unknown as the Standard Model (SM) of particle physics fails to provide a viable dark matter (DM) candidate. Despite

* Corresponding authors.

E-mail addresses: chensl@mail.ccnu.edu.cn (S.-L. Chen), amitdbanik@mail.ccnu.edu.cn (A. Dutta Banik), zekunliu@mails.ccnu.edu.cn (Z.-K. Liu).

<https://doi.org/10.1016/j.nuclphysb.2021.115394>

0550-3213/© 2021 Published by Elsevier B.V. This is an open access article under the CC BY license

(<http://creativecommons.org/licenses/by/4.0/>). Funded by SCOAP³.

being celebrated as the most successful theory after the discovery of Higgs boson at collider experiments, various theories beyond the SM are proposed in order to explain the dark matter. Simple extensions of SM with DM candidate are probed considering the stability of dark matter is protected by an additional discrete symmetry (such as \mathcal{Z}_2 or \mathcal{Z}_3 etc.). Apart from the dark matter, the origin of neutrino mass also remains unexplained by the SM of particle physics despite various neutrinos oscillation experiments has confirmed that neutrinos are massive [2]. This discrepancy in SM also calls for theories beyond the SM. Neutrino masses can indeed be generated by various see-saw mechanisms [3–13] at tree level with new heavy fermions and scalar fields, which can also generate matter-antimatter asymmetry in the Universe through the leptogenesis mechanism [14–18]. There are alternative ways to generate neutrino masses and matter-antimatter asymmetry where neutrino mass is generated radiatively via loop involving right-handed neutrinos [19–22] or new fields [23–28], which can also provide viable dark matter candidates.

Among various extensions beyond the SM, two Higgs doublet model (2HDM) is one of the most simplest extensions where an additional scalar doublet similar to SM Higgs doublet is added [29–32]. In conventional models of 2HDM, the newly added doublet is assumed to be odd under a \mathcal{Z}_2 symmetry which is broken spontaneously after electroweak symmetry is broken. After spontaneous symmetry breaking (SSB) doublet scalar fields obtain vacuum expectation values (VEVs) and mix up, resulting new physical Higgs particles. In the present work, we explore the phenomenology of a 2HDM extended Georgi-Machacek (GM) model [33–35]. In the GM model, new scalar triplets with hypercharge $Y = 0$ and $Y = 1$ are added to the SM scalar sector in a way that the electroweak ρ -parameter remains unaffected by simply assuming both the triplets develop same VEVs after spontaneous breaking of symmetry [36–40]. The hypercharge $Y = 1$ triplet in GM model also produces tiny neutrino masses at tree level. We propose an extension of the GM model with an additional scalar doublet and new vector-like fermions charged under $SU(2)_L \times U(1)_Y \times \mathcal{Z}_4 \times \mathcal{Z}_2$ symmetry. After spontaneous breaking of the symmetry, both the doublet scalar fields develop VEVs resembling the usual 2HDM (which breaks \mathcal{Z}_4 symmetry of the model) while the triplet fields and vector fermion doublets remain protected by the imposed \mathcal{Z}_2 which constitutes the dark sector. The neutrino mass generation at tree level via triplet field is prohibited. However, new vector-like fermions provide a window to radiatively generate neutrino mass in one-loop level. In addition, the lightest neutral scalar particle arising from mixing between triplet fields being charged under the remnant \mathcal{Z}_2 , is stable and serves as a dark matter candidate. Finally, CP violating decays of heavy vector fermions can explain the matter-antimatter asymmetry in the Universe via leptogenesis. With new scalar and fermion fields the modified GM model is referred as scotogenic Georgi-Machacek (sGM) model.

The paper is organized as follows, we firstly describe the sGM model in detail. The phenomenologies of the model are then performed with considering various theoretical and experimental limits. Study of leptogenesis within the model is presented in the next section. Finally we conclude the paper.

2. sGM model

The scalar sector of the GM model [33] contains one Higgs doublet ϕ with $Y = 1/2$, one complex triplet Δ with $Y = 1$ and a real scalar triplet T with $Y = 0$ fields.

$$\phi = \begin{pmatrix} \phi^+ \\ \phi^0 \end{pmatrix}, \quad \Delta = \begin{pmatrix} \frac{D^+}{\sqrt{2}} & -D^{++} \\ D^0 & -\frac{D^+}{\sqrt{2}} \end{pmatrix}, \quad T = \begin{pmatrix} \frac{T^0}{\sqrt{2}} & -T^+ \\ -T^- & -\frac{T^0}{\sqrt{2}} \end{pmatrix}, \quad (1)$$

Table 1
Charge assignments of the fields in the sGM model.

Fields	$SU(3)_c$	$SU(2)_L$	$U(1)_Y$	\mathcal{Z}_4	\mathcal{Z}_2
T	1	3	0	1	-
Δ	1	3	1	1	-
ϕ_1	1	2	1/2	-i	+
ϕ_2	1	2	1/2	i	+
$\Sigma_{L,R}$	1	2	-1/2	1	-
Q_L	3	1	1/6	1	+
u_R	3	1	2/3	i	+
d_R	3	1	-1/3	-i	+
L_L	1	2	-1/2	1	+
e_R	3	1	-1	-i	+

where the neutral components are parametrized as

$$\phi^0 = \frac{1}{\sqrt{2}}(\phi_r + v_\phi + i\phi_i), \quad D^0 = \frac{1}{\sqrt{2}}(D_r^0 + iD_i^0) + v_\Delta, \quad T^0 = T_r + v_T, \quad (2)$$

with v_ϕ , v_Δ and v_T being the VEVs for ϕ^0 , D^0 and T^0 , respectively. The most general form of the Higgs potential, invariant under the $SU(2)_L \times U(1)_Y$ gauge symmetry, is given by

$$\begin{aligned} V(\phi, \Delta, T) = & m_\phi^2(\phi^\dagger\phi) + m_\Delta^2\text{Tr}(\Delta^\dagger\Delta) + \frac{m_T^2}{2}\text{Tr}(T^2) \\ & + \mu_1\phi^\dagger T\phi + \mu_2[\phi^T(i\tau_2)\Delta^\dagger\phi + \text{h.c.}] + \mu_3\text{Tr}(\Delta^\dagger\Delta T) + \lambda_\phi(\phi^\dagger\phi)^2 \\ & + \rho_1[\text{Tr}(\Delta^\dagger\Delta)]^2 + \rho_2\text{Tr}(\Delta^\dagger\Delta\Delta^\dagger\Delta) + \rho_3\text{Tr}(T^4) + \rho_4\text{Tr}(\Delta^\dagger\Delta)\text{Tr}(T^2) \\ & + \rho_5\text{Tr}(\Delta^\dagger T)\text{Tr}(T\Delta) \\ & + \kappa_1\text{Tr}(\Delta^\dagger\Delta)\phi^\dagger\phi + \kappa_2\phi^\dagger\Delta\Delta^\dagger\phi + \frac{\kappa_3}{2}\text{Tr}(T^2)\phi^\dagger\phi + \kappa(\phi^\dagger\Delta T\tilde{\phi} + \text{h.c.}), \quad (3) \end{aligned}$$

where $\tilde{\phi} = i\tau_2\phi^*$. In the above Eq. (3), μ_2 and κ can be complex.

In the present work we extend the model in the framework of two Higgs doublets with vector-like fermions (VLF's),

$$\Sigma_L \equiv (\Sigma_L^0 \quad \Sigma_L^-)^T, \quad \Sigma_R \equiv (\Sigma_R^0 \quad \Sigma_R^-)^T. \quad (4)$$

We consider a \mathcal{Z}_4 symmetry associated with the model instead of standard \mathcal{Z}_2 symmetry in 2HDM. In addition, we introduce a \mathcal{Z}_2 symmetry under which both the triplets and vector fermion doublets are odd which constitute the dark sector. Charges of different particles and fields are given in Table 1.

The general form of the Higgs potential, invariant under the $SU(2)_L \times U(1)_Y \times \mathcal{Z}_4 \times \mathcal{Z}_2$ symmetry, is parametrized as

$$\begin{aligned} V(2\text{HDM}, \Delta, T) = & V_{2\text{HDM}} + m_\Delta^2\text{Tr}(\Delta^\dagger\Delta) + \frac{m_T^2}{2}\text{Tr}(T^2) \\ & + \rho_1[\text{Tr}(\Delta^\dagger\Delta)]^2 + \rho_2\text{Tr}(\Delta^\dagger\Delta\Delta^\dagger\Delta) + \rho_3\text{Tr}(T^4) + \rho_4\text{Tr}(\Delta^\dagger\Delta)\text{Tr}(T^2) \\ & + \rho_5\text{Tr}(\Delta^\dagger T)\text{Tr}(T\Delta) \\ & + \sum_{a=1,2} \left(\kappa_{1a}\text{Tr}(\Delta^\dagger\Delta)\phi_a^\dagger\phi_a + \kappa_{2a}\phi_a^\dagger\Delta\Delta^\dagger\phi_a + \frac{\kappa_{3a}}{2}\text{Tr}(T^2)\phi_a^\dagger\phi_a \right) \\ & + \kappa_{41}(\phi_1^\dagger\Delta T\tilde{\phi}_2 + \text{h.c.}) + \kappa_{42}(\phi_2^\dagger\Delta T\tilde{\phi}_1 + \text{h.c.}), \quad (5) \end{aligned}$$

where $\tilde{\phi}_{1,2} \equiv i\tau_2\phi_{1,2}^*$, and the 2HDM potential is given by

$$V_{2\text{HDM}} = m_{11}^2 \phi_1^\dagger \phi_1 + m_{22}^2 \phi_2^\dagger \phi_2 + \frac{\lambda_1}{2} (\phi_1^\dagger \phi_1)^2 + \frac{\lambda_2}{2} (\phi_2^\dagger \phi_2)^2 + \lambda_3 \phi_1^\dagger \phi_1 \phi_2^\dagger \phi_2 \\ + \lambda_4 \phi_1^\dagger \phi_2 \phi_2^\dagger \phi_1 + \frac{\lambda_5}{2} \left[(\phi_1^\dagger \phi_2)^2 + (\phi_2^\dagger \phi_1)^2 \right]. \quad (6)$$

One interesting aspect of the choice \mathcal{Z}_4 is that it forbids interaction terms $\phi_1^\dagger \Delta T \tilde{\phi}_1$ and $\phi_2^\dagger \Delta T \tilde{\phi}_2$ in Eq. (5) and the soft breaking term $m_{12}^2 \phi_1^\dagger \phi_2$ in 2HDM potential (Eq. (6)). However new interactions in Eq. (5) are allowed with coupling $\kappa_{41,42}$ which play significant role in generation of neutrino mass, as we will show later. The \mathcal{Z}_4 symmetry is broken spontaneously as the doublet fields ϕ_1, ϕ_2 acquires VEVs. However, triplet fields in the potential expression of Eq. (5) preserves the \mathcal{Z}_2 symmetry ($T \rightarrow -T$ and $\Delta \rightarrow -\Delta$ following Table 1) and does not acquire any VEV. Therefore, this remnant \mathcal{Z}_2 symmetry provides feasible candidates for dark matter arising from the mixing between neutral components of triplet fields in the model. After spontaneous breaking of symmetry we get new physical scalar in visible 2HDM sector and a dark sector originating from triplet scalars. The neutral scalar particles and singly charged particles of the triplets T and Δ mix with each other and provides two neutral physical scalars and two physical charged scalars in dark sector. However, since the VEV of Δ field is zero due to the residual symmetry \mathcal{Z}_2 , the neutrino mass is vanishing at tree level in the model. This issue can be resolved by the newly added vector-like fermions which also respects the unbroken \mathcal{Z}_2 symmetry.

Gauge invariant Yukawa interactions of the fermions with triplet scalars in the present framework are given as

$$\mathcal{L} = M_\Sigma \bar{\Sigma}_L \Sigma_R + y \bar{L}_L^c i\tau_2 \Delta \Sigma_L + \lambda \bar{L}_L T \Sigma_R + \text{h.c.} . \quad (7)$$

We will later show that these new interaction terms provide necessary ingredients to radiatively generate neutrino masses in one-loop.

2.1. Scalar sector

After spontaneous symmetry breaking, Higgs fields ϕ_1 and ϕ_2 acquire vacuum expectation values v_1 and v_2 , such that $v = \sqrt{v_1^2 + v_2^2} = 246$ GeV. The visible sector is identical to 2HDM which contains two neutral physical scalars (h, H), one pseudo-scalar particle A and a pair of charged scalar H^\pm . Conditions for the minimization of the potential are

$$m_{11}^2 = \frac{-\lambda_1 v_1^2 - (\lambda_3 + \lambda_4 + \lambda_5) v_2^2}{2}, \\ m_{22}^2 = \frac{-\lambda_2 v_2^2 - (\lambda_3 + \lambda_4 + \lambda_5) v_1^2}{2}. \quad (8)$$

Different couplings λ_i ($i = 1, \dots, 5$) are expressed in terms of physical masses m_h, m_H, m_A, m_{H^\pm} and parameters α, β ,

$$\lambda_1 = \frac{1}{v^2 c_\beta^2} \left(c_\alpha^2 m_H^2 + s_\alpha^2 m_h^2 \right), \quad (9)$$

$$\lambda_2 = \frac{1}{v^2 s_\beta^2} \left(s_\alpha^2 m_H^2 + c_\alpha^2 m_h^2 \right), \quad (10)$$

$$\lambda_4 = \frac{1}{v^2} (m_A^2 - 2m_{H^+}^2), \tag{11}$$

$$\lambda_5 = -\frac{m_A^2}{v^2}, \tag{12}$$

$$\lambda_3 = \frac{1}{v^2 s_\beta c_\beta} \left((m_H^2 - m_h^2) s_\alpha c_\alpha + m_A^2 s_\beta c_\beta \right) - \lambda_4, \tag{13}$$

where we denote $s_{\alpha,\beta} = \sin \alpha, \sin \beta$, $c_{\alpha,\beta} = \cos \alpha, \cos \beta$, with $\tan \beta = v_2/v_1$. Here $m_h = 125$ GeV is the mass of SM Higgs and m_H is denoted as the mass of heavy Higgs boson. After the SSB, the scalar fields T and Δ acquire zero VEVs which resemble an unbroken residual \mathcal{Z}_2 symmetry. Therefore, the scalar fields T and Δ are inert in nature. Mass terms for different inert scalar particles are given as follows

$$\begin{aligned} m_{T^0}^2 &= M_T^2 + \frac{1}{2} \kappa_{31} v_1^2 + \frac{1}{2} \kappa_{32} v_2^2 = m_{T^+}^2, \\ m_{D^0}^2 &= M_\Delta^2 + \frac{1}{2} (\kappa_{11} + \kappa_{21}) v_1^2 + \frac{1}{2} (\kappa_{12} + \kappa_{22}) v_2^2 = m_{A^0}^2, \\ m_{D^{++}}^2 &= M_\Delta^2 + \frac{1}{2} \kappa_{11} v_1^2 + \frac{1}{2} \kappa_{12} v_2^2, \\ m_{D^+}^2 &= M_\Delta^2 + \frac{1}{2} (\kappa_{11} + \frac{1}{2} \kappa_{21}) v_1^2 + \frac{1}{2} (\kappa_{12} + \frac{1}{2} \kappa_{22}) v_2^2, \\ m_{TD}^2 &= -\left(\frac{\kappa_{41} v_1 v_2}{2} + \frac{\kappa_{42} v_1 v_2}{2} \right), \\ m_{T^+ D^+}^2 &= \frac{\kappa_{41} v_1 v_2}{2\sqrt{2}} + \frac{\kappa_{42} v_1 v_2}{2\sqrt{2}}. \end{aligned} \tag{14}$$

The mass of inert pseudo-scalar is denoted as m_{A^0} and $m_{D^{++}}$ is the mass of doubly charged scalar. Neutral parts of both the triplets mix with each other resulting two new physical neutral scalars $S_{1,2}$ and the mass matrix is given as

$$M_{neutral}^2 = \begin{pmatrix} m_{T^0}^2 & m_{TD}^2 \\ m_{TD}^2 & m_{D^0}^2 \end{pmatrix}. \tag{15}$$

We define a mixing angle γ between these two inert scalar fields such that

$$\begin{aligned} S_1 &= T^0 \cos \gamma - D_r^0 \sin \gamma, \\ S_2 &= T^0 \sin \gamma + D_r^0 \cos \gamma. \end{aligned} \tag{16}$$

Masses of new physical scalars are expressed as

$$m_{S_1/S_2}^2 = \frac{m_{T^0}^2 + m_{D^0}^2}{2} \mp \frac{m_{D^0}^2 - m_{T^0}^2}{2} \sqrt{1 + x^2}, \tag{17}$$

where $x = \tan 2\gamma = \frac{2m_{TD}^2}{(m_{D^0}^2 - m_{T^0}^2)}$. Similarly, the charged parts also mix with each other and provides two physical charged scalars $S_{1,2}^+$. The mass matrix for the charged scalars is

$$M_{charged}^2 = \begin{pmatrix} m_{T^+}^2 & m_{T^+ D^+}^2 \\ m_{T^+ D^+}^2 & m_{D^+}^2 \end{pmatrix}. \tag{18}$$

Defining a new mixing angle δ , we write physical charged scalars as

$$\begin{aligned}
 S_1^+ &= T^+ \cos \delta - D^+ \sin \delta, \\
 S_2^+ &= T^+ \sin \delta + D^+ \cos \delta.
 \end{aligned}
 \tag{19}$$

Masses of physical charged scalars are

$$m_{S_1^+/S_2^+}^2 = \frac{m_{T^+}^2 + m_{D^+}^2}{2} \mp \frac{m_{D^+}^2 - m_{T^+}^2}{2} \sqrt{1 + y^2},
 \tag{20}$$

with $y = \tan 2\delta = \frac{2m_{T^+D^+}^2}{(m_{D^+}^2 - m_{T^+}^2)}$.

2.2. Vacuum stability

We adopt the criteria of copositivity of symmetric matrices to get the conditions of vacuum stability [41]. Only the quartic terms in the potential should be considered, since these terms dominate at large field value. It is to be noted that vacuum stability conditions don't give any constraints to couplings κ_{41} and κ_{42} . This is because we can make these couplings positive by applying a phase rotation of a field or field redefinition. We parameterize the fields as,

$$\begin{aligned}
 \phi_1^\dagger \phi_1 &= |h_1|^2 & \phi_2^\dagger \phi_2 &= |h_2|^2 & \Delta^\dagger \Delta &= |\delta|^2 & T^\dagger T &= |t|^2 & \phi_1^\dagger \phi_2 &= f |h_1| |h_2| e^{i\theta_1} \\
 \Delta^\dagger T &= g |\delta| |t| e^{i\theta_2} & \Delta^\dagger \phi_1 &= m |\delta| |\phi_1| e^{i\theta_3} & \Delta^\dagger \phi_2 &= n |\delta| |\phi_2| e^{i\theta_4}
 \end{aligned}
 \tag{21}$$

where $f, g, m, n \in [0, 1]$. According to the definition above, considering the quartic terms out and ignoring κ_{41} and κ_{42} terms, the potential of Eq. (5) can be expressed as

$$\begin{aligned}
 V(h_1, h_2, \delta, t) &= \frac{\lambda_1}{2} h_1^4 + \frac{\lambda_2}{2} h_2^4 + \lambda_3 h_1^2 h_2^2 + \lambda_4 \rho^2 h_1^2 h_2^2 + \frac{\lambda_5}{2} f^2 \cos 2\theta_1 h_1^2 h_2^2 \\
 &\quad + (\rho_1 + \rho_2) \delta^4 + \rho_3 t^4 + (\rho_4 + \rho_5 g^2) \delta^2 t^2 + (\kappa_{11} + \kappa_{21} m^2) \delta^2 h_1^2 \\
 &\quad + \frac{\kappa_{31}}{2} t^2 h_1^2 + (\kappa_{11} + \kappa_{22} n^2) \delta^2 h_2^2 + \frac{\kappa_{32}}{2} t^2 h_2^2
 \end{aligned}
 \tag{22}$$

The symmetric matrix of quartic couplings can be represented in basis $(h_1^2, h_2^2, \delta^2, t^2)$ as

$$M = \begin{pmatrix} \frac{1}{2}\lambda_1 & \frac{1}{2}\lambda_{345} & \frac{1}{2}(\kappa_{11} + m^2\kappa_{21}) & \frac{1}{4}\kappa_{31} \\ & \frac{1}{2}\lambda_2 & \frac{1}{2}(\kappa_{12} + n^2\kappa_{22}) & \frac{1}{4}\kappa_{32} \\ & & \rho_1 + \rho_2 & \frac{1}{2}(\rho_4 + g^2\rho_5) \\ & & & \rho_3 \end{pmatrix}
 \tag{23}$$

where $\lambda_{345} = \lambda_3 + f^2(\lambda_4 - |\lambda_5|)$. If $(\lambda_4 - |\lambda_5|) \geq 0$, the minimum of the potential is obtained for $f = 0$, whereas for $(\lambda_4 - |\lambda_5|) < 0$ the minimum obtained assuming $f = 1$. Similar convention can be employed to parameters g, m, n to apply the copositivity criteria upon the matrix M . Copositive conditions for which vacuum of the scalar potential in Eq. (22) becomes stable are:

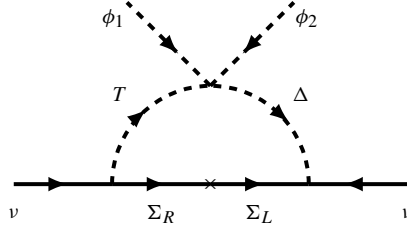


Fig. 1. One-loop neutrino mass in sGM model.

$$\begin{aligned}
 &\lambda_1 \geq 0, \quad \lambda_2 \geq 0, \quad \rho_1 + \rho_2 \geq 0, \quad \rho_3 \geq 0, \\
 &\kappa_{11} + \kappa_{21} + \sqrt{2\lambda_1(\rho_1 + \rho_2)} \geq 0, \\
 &\kappa_{11} + \sqrt{2\lambda_1(\rho_1 + \rho_2)} \geq 0, \\
 &\kappa_{12} + \kappa_{22} + \sqrt{2\lambda_1(\rho_1 + \rho_2)} \geq 0, \\
 &\kappa_{12} + \sqrt{2\lambda_1(\rho_1 + \rho_2)} \geq 0, \\
 &\lambda_3 + \lambda_4 - |\lambda_5| + \sqrt{\lambda_1\lambda_2} \geq 0, \\
 &\lambda_3 + \sqrt{\lambda_1\lambda_2} \geq 0, \\
 &8\lambda_1\rho_3 - \kappa_{31}^2 \geq 0, \\
 &8\lambda_2\rho_3 - \kappa_{32}^2 \geq 0, \\
 &8(\lambda_3 + \lambda_4 - |\lambda_5|)\rho_3 - \kappa_{31}\kappa_{32} + 2\sqrt{(8\lambda_1\rho_3 - \kappa_{31}^2)(8\lambda_2\rho_3 - \kappa_{32}^2)} \geq 0, \\
 &8\lambda_3\rho_3 - \kappa_{31}\kappa_{32} + 2\sqrt{(8\lambda_1\rho_3 - \kappa_{31}^2)(8\lambda_2\rho_3 - \kappa_{32}^2)} \geq 0,
 \end{aligned} \tag{24}$$

where we used a theorem of copositivity criteria to get copositive matrix conditions [42]. The conditions mentioned above are derived assuming $\rho_4 \geq 0$ and $\rho_5 \geq 0$.

In addition, scalar and fermion couplings must also remain within the perturbative limit for which following conditions must be satisfied

$$\lambda_i, \kappa_{1i,2i,3i,4i}, \rho_i < 4\pi, \quad \lambda, y < \sqrt{4\pi}. \tag{25}$$

2.3. Neutrino mass

The neutrino masses are generated via one-loop diagram as shown in Fig. 1. The Yukawa interaction terms in Eq. (7) and scalar terms with κ_{41} and κ_{42} appearing in Eq. (5) are responsible for generation of light neutrino mass. The \mathcal{Z}_4 symmetry in the model assures that two different scalar doublets are necessary in order to generate tiny neutrino mass in one-loop.

Neutrino mass in the present model can further be realized as self-energy corrections. However, there will be contributions from two different diagrams involving neutral scalars and charged scalars as shown in Fig. 2. The expression of neutrino mass is given as

$$\begin{aligned}
 (\mathcal{M}_\nu)_{ij} &= \cos \gamma \sin \gamma \sum_{k=1}^3 \frac{[y_{ik}\lambda_{jk} + \lambda_{ik}y_{jk}]}{32\pi^2} \\
 &\times M_{\Sigma_k} \left[\frac{m_{S_1}^2}{m_{S_1}^2 - M_{\Sigma_k}^2} \ln \frac{m_{S_1}^2}{M_{\Sigma_k}^2} - \frac{m_{S_2}^2}{m_{S_2}^2 - M_{\Sigma_k}^2} \ln \frac{m_{S_2}^2}{M_{\Sigma_k}^2} \right]
 \end{aligned}$$

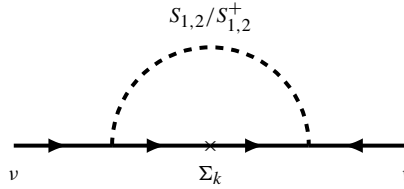


Fig. 2. Neutrino mass from self energy diagrams.

$$\begin{aligned}
 & -\cos \delta \sin \delta \sum_{k=1}^3 \frac{[y_{ik}\lambda_{jk} + \lambda_{ik}y_{jk}]}{32\pi^2} \\
 & \times M_{\Sigma_k} \left[\frac{m_{S_1^+}^2}{m_{S_1^+}^2 - M_{\Sigma_k}^2} \ln \frac{m_{S_1^+}^2}{M_{\Sigma_k}^2} - \frac{m_{S_2^+}^2}{m_{S_2^+}^2 - M_{\Sigma_k}^2} \ln \frac{m_{S_2^+}^2}{M_{\Sigma_k}^2} \right]. \tag{26}
 \end{aligned}$$

It is to be noted that, in the present scenario if the mixing angle between neutral physical scalar $\sin \gamma \rightarrow 0$, then mixing angle between charged scalars ($\sin \delta$) also becomes zero. The conditions for which those mixing angles become zero are

$$\kappa_{41} = \kappa_{42} = 0, \quad \kappa_{41} = -\kappa_{42}. \tag{27}$$

Therefore, in order to generate tiny neutrino mass one must have $\kappa_{41,42} \neq 0$ and $\kappa_{41} \neq -\kappa_{42}$.

We consider vector fermions to be much heavier than scalar particles $M_{\Sigma} \gg m_{S_{1,2}}, m_{S_{1,2}^+}$, and further assume $m_{S_1^+}^2 \simeq m_{S_2^+}^2, m_{S_1^+}^2 \simeq m_{S_2^+}^2$. With the above simplified choice, following Eqs. (14), (17) and Eq. (20) we can rewrite the neutrino mass matrix elements as

$$\begin{aligned}
 (\mathcal{M}_\nu)_{ij} &= \left(\frac{\kappa_{41} + \kappa_{42}}{2} \right) v_1 v_2 \left[\sum_{k=1}^3 \frac{[y_{ik}\lambda_{jk} + \lambda_{ik}y_{jk}]}{32\pi^2} \frac{1}{M_{\Sigma_k}} \ln \frac{m_{S_1^+}^2}{M_{\Sigma_k}^2} \right. \\
 & \left. + \sum_{k=1}^3 \frac{[y_{ik}\lambda_{jk} + \lambda_{ik}y_{jk}]}{32\pi^2} \frac{1}{\sqrt{2}M_{\Sigma_k}} \ln \frac{m_{S_1^+}^2}{M_{\Sigma_k}^2} \right]. \tag{28}
 \end{aligned}$$

Therefore, from Eq. (28), one can realize seesaw like radiative neutrino mass expressed as

$$\mathcal{M}_\nu = \frac{(2 + \sqrt{2})(\kappa_{41} + \kappa_{42})v_1 v_2}{128\pi^2} (y\zeta^{-1}\lambda^T + \lambda\zeta^{-1}y^T), \tag{29}$$

where we assumed that the mass matrix of vector fermion $\zeta = \text{diag}\{\zeta_1, \zeta_2, \zeta_3\}$ and the diagonal matrix elements are given as

$$\zeta_i \equiv M_{\Sigma_i} \left[\ln \frac{m_{S_1^+}^2}{M_{\Sigma_i}^2} \right]^{-1} = M_{\Sigma_i} \left[\ln \frac{m_{S_1^+}^2}{M_{\Sigma_i}^2} \right]^{-1}. \tag{30}$$

Therefore, if one considers $(\kappa_{41} + \kappa_{42}) \sim \mathcal{O}(1)$, $y \sim \lambda \simeq \mathcal{O}(10^{-2})$, $\tan \beta \sim 1$ and $M_{\Sigma} \sim \mathcal{O}(10^{10})$ GeV, we get neutrino mass scale at $m_\nu \simeq \mathcal{O}(0.05)$ eV for TeV scale triplets in sGM framework. The order of Yukawa coupling also controls parameters significant for the process of leptogenesis which will be discussed later. The mass matrix \mathcal{M}_ν can be diagonalized by Pontecorvo-Maki-Nakagawa-Sakata (PMNS) matrix U

$$\mathcal{M}_\nu = U^* \cdot \hat{\mathcal{M}}_\nu \cdot U^\dagger \quad (31)$$

where $\hat{\mathcal{M}}_\nu = \text{diag}(m_1, m_2, m_3)$.

3. Theory and phenomenology of the sGM model

3.1. Electroweak precision test observables

We consider the generalised form of GM model (Eq. (5)) since it is well known that custodial symmetry in GM model is broken at the one-loop level by hypercharge interactions [43–45]. After symmetries of the scalar potential breaks spontaneously, \mathcal{Z}_2 symmetry is partially conserved by triplet scalars and both $Y = 0$ and $Y = 1$ triplet fields remain inert. At this stage (after SSB), Higgs doublets and new inert triplets doesn't have any impact on ρ parameter and $\rho = 1$ is satisfied at tree level. However, one-loop corrections parameter to ρ parameter must be taken into account which can also be obtained in terms of $\bar{T} = \alpha T = \Delta\rho$ due to new scalars and fermions. Firstly, let us consider the contribution from new fermions within the model. For a single generation of vector doublet fermions, there will be new contribution to \bar{T} parameter which is given as [46]

$$\bar{T}^{\text{VLF}} = -\frac{g_2^2}{8\pi^2 m_W^2} \Pi(m_1, m_2), \quad (32)$$

where

$$\begin{aligned} \Pi(m_1, m_2) = & -\frac{1}{2} (m_1^2 + m_2^2) \left(\text{div} + \log \left(\frac{\mu_{EW}^2}{m_1 m_2} \right) \right) \\ & + m_1 m_2 \left(\text{div} + \frac{(m_1^2 + m_2^2) \log \left(\frac{m_2^2}{m_1^2} \right)}{2(m_1^2 - m_2^2)} + \log \left(\frac{\mu_{EW}^2}{m_1 m_2} \right) + 1 \right) \\ & - \frac{1}{4} (m_1^2 + m_2^2) - \frac{(m_1^4 + m_2^4) \log \left(\frac{m_2^2}{m_1^2} \right)}{4(m_1^2 - m_2^2)}. \end{aligned} \quad (33)$$

In the present work we include three vector fermion doublets. However, since vector fermions do not mix with each other and mass of charged and neutral fermions are degenerate (i.e.; $M_{\Sigma^+} = M_{\Sigma^0} = M_\Sigma$ for a single generation), the contribution $\bar{T}^{\text{VLF}} = 0$.

Let us now discuss how electroweak precision observables modify in presence of new scalars. In case of 2HDM within alignment limit ($\beta - \alpha = \pi/2$), contribution to \bar{T} parameter reads as [47–49]

$$\bar{T}^{\text{2HDM}} = \frac{g_2^2}{64\pi^2 m_W^2} \left(\xi \left(m_{H^\pm}^2, m_A^2 \right) + \xi \left(m_{H^\pm}^2, m_H^2 \right) - \xi \left(m_A^2, m_H^2 \right) \right), \quad (34)$$

where

$$\xi(x, y) = \begin{cases} \frac{x+y}{2} - \frac{xy}{x-y} \ln \left(\frac{x}{y} \right), & \text{if } x \neq y. \\ 0, & \text{if } x = y. \end{cases} \quad (35)$$

From Eq. (34), it can be concluded that $\bar{T}^{2\text{HDM}}$ vanishes for $m_A = m_{H^\pm}$ or $m_H = m_{H^\pm}$. Therefore, if one considers above conditions, new contribution to \bar{T} parameter will arise from triplet scalar fields T and Δ only. It is to noted that, in the present formalism there exists mixing between neutral and charged components of the triplet fields, which must be taken into account to calculate \bar{T} . Considering the effects of mixing, additional contribution to \bar{T} parameter is

$$\begin{aligned} \bar{T}^{new} = & \frac{g_2^2}{64\pi^2 m_W^2} \left(s_\delta^2 \xi(m_{D^{\pm\pm}}^2, m_{S_1^\pm}^2) + c_\delta^2 \xi(m_{D^{\pm\pm}}^2, m_{S_2^\pm}^2) \right. \\ & + (c_\delta s_\gamma / \sqrt{2} + c_\gamma s_\delta)^2 \xi(m_{S_2^\pm}^2, m_{S_1^\pm}^2) + (c_\delta c_\gamma / \sqrt{2} - s_\gamma s_\delta)^2 \xi(m_{S_2^\pm}^2, m_{S_2^\pm}^2) \\ & + (s_\delta s_\gamma / \sqrt{2} - c_\gamma c_\delta)^2 \xi(m_{S_1^\pm}^2, m_{S_1^\pm}^2) + (s_\delta c_\gamma / \sqrt{2} + s_\gamma c_\delta)^2 \xi(m_{S_2^\pm}^2, m_{S_1^\pm}^2) \\ & + s_\delta^2 \xi(m_{S_1^\pm}^2, m_{A^0}^2) / 2 + c_\delta^2 \xi(m_{S_2^\pm}^2, m_{A^0}^2) / 2 - 2s_\delta^2 c_\delta^2 \xi(m_{S_2^\pm}^2, m_{S_1^\pm}^2) \\ & \left. - c_\gamma^2 \xi(m_{S_2^\pm}^2, m_{A^0}^2) - s_\gamma^2 \xi(m_{S_1^\pm}^2, m_{A^0}^2) \right). \end{aligned} \tag{36}$$

In the above Eq. (36), $s_\theta = \sin \theta$ and $c_\theta = \cos \theta$ where $\theta = \gamma, \delta$. Using the above expression, bounds on the mixing angles or mass splittings between scalar particles can be obtained in the present model. We use the value $T = \frac{\bar{T}^{new}}{\alpha} = 0.07 \pm 0.12$ [2] to constrain the model parameter space.

3.2. Collider bounds

In this section, we briefly discuss collider constraints on different visible and dark sector particles of the model. LEP excludes a new charged scalar of mass less than 80 GeV from charged scalar decay into cs and $\nu\tau$ final state [50]. Similarly bound on charged fermion mass is 101.2 GeV [51,52] from the decay of charged fermion into νW^\pm final state. Let us now consider the bounds obtained from LHC. In the present model we have singly charged scalars $S_{1,2}^\pm$ and one doubly charged scalar $D^{\pm\pm}$ in dark sector. These particles can contribute to the Higgs to diphoton decay process. The decay rate for the process $h \rightarrow \gamma\gamma$ is given as

$$\begin{aligned} \Gamma(h \rightarrow \gamma\gamma) = & \frac{\alpha^2 G_F m_h^3}{128 \sqrt{2} \pi^3} \left| \sum_f N_c Q_f^2 g_{hf\bar{f}} A_{1/2}^h(\tau_f) + g_{hW^+W^-} A_1^h(\tau_W) \right. \\ & + \frac{\lambda_{hH^\pm H^\mp} v}{2m_{H^\pm}^2} A_0^h(\tau_{H^\pm}) + \frac{\lambda_{hS_1^\pm S_1^\mp} v}{2m_{S_1^\pm}^2} A_0^h(\tau_{S_1^\pm}) + \frac{\lambda_{hS_2^\pm S_2^\mp} v}{2m_{S_2^\pm}^2} A_0^h(\tau_{S_2^\pm}) \\ & \left. + 4 \frac{\lambda_{hD^{\pm\pm} D^{\mp\mp}} v}{2m_{D^{\pm\pm}}^2} A_0^h(\tau_{D^{\pm\pm}}) \right|^2. \end{aligned} \tag{37}$$

Here G_F is the Fermi coupling constant, α is the fine-structure constant, $N_c = 3(1)$ for quarks (leptons), Q_f is the electric charge of the fermion in the loop, and $\tau_i = m_h^2 / 4m_i^2$ ($i = f, W, S_1^\pm, H^\pm, S_2^\pm, D^{\pm\pm}$). Couplings of SM Higgs h with different charged scalars in Eq. (37) are listed in Appendix. The relevant loop functions are given by

$$A_{1/2}^h(\tau) = 2[\tau + (\tau - 1)f(\tau)]\tau^{-2}, \tag{38}$$

$$A_1^h(\tau) = -[2\tau^2 + 3\tau + 3(2\tau - 1)f(\tau)]\tau^{-2}, \tag{39}$$

$$A_0^h(\tau) = -[\tau - f(\tau)]\tau^{-2}, \tag{40}$$

and the function $f(\tau)$ is given by

$$f(\tau) = \begin{cases} \left[\sin^{-1}(\sqrt{\tau}) \right]^2, & (\tau \leq 1), \\ -\frac{1}{4} \left[\log \left(\frac{1 + \sqrt{1 - \tau^{-1}}}{1 - \sqrt{1 - \tau^{-1}}} \right) - i\pi \right]^2, & (\tau > 1). \end{cases} \quad (41)$$

One can calculate the quantity called signal strength $R_{\gamma\gamma}$ given as

$$R_{\gamma\gamma} = \frac{\sigma(pp \rightarrow h) Br(h \rightarrow \gamma\gamma)}{\sigma(pp \rightarrow h)^{\text{SM}} Br(h \rightarrow \gamma\gamma)^{\text{SM}}} \quad (42)$$

Using the latest and future constraints from LHC on the $R_{\gamma\gamma}$ signal strength [53,54], masses of charged particles in our model can be constrained. It is to be noted that for heavier masses of charged inert scalar particles with mass around TeV, one can safely work with 2HDM constraints. In the present framework, we consider only one Higgs doublet ϕ_2 couples to the SM sector which resembles the standard type-I 2HDM. For type-I 2HDM, Higgs signal strength does not provide any limit on $\tan\beta$ with alignment limit $(\beta - \alpha) = \pi/2$. However, deviation from the alignment limit puts stringent bound on $\tan\beta$ for type-I 2HDM [55–58]. Apart from Higgs signal strength measurement, the most stringent bound on charged scalar mass comes from flavor physics when the $B \rightarrow X_s \gamma$ decay is taken into account [59,60]. It is found that for all types of 2HDM including type-I 2HDM, inclusive decay $b \rightarrow s \gamma$ excludes charged Higgs mass below 650 GeV for $\tan\beta < 1$ [60]. Therefore, in the present framework, with the alignment limit $(\beta - \alpha) = \pi/2$, we conservatively work with following conditions

$$m_H = 500 \text{ GeV}, m_A = m_{H^\pm} = 650 \text{ GeV}, 1 \leq \tan\beta \leq 10. \quad (43)$$

3.3. Dark matter

As mentioned before, the lightest neutral scalar S_1 or S_2 can serve the role of dark matter candidate in the model. We implement the model in LanHEP-3.3.2 [61] and calculate relic density and direct detection of the dark matter using micrOMEGAS-4.3.5 [62]. We use the dark matter relic density observed by PLANCK [1] and constrain the model with the dark matter-nucleon scattering cross-section limits from direct search experiments XENON1T [63,64] and PandaX-II [65,66].

Apart from 2HDM parameters (as in Eq. (43)), there are dark sector parameters in the model. We consider the following parameters to be independent parameters which constrain the dark sector in the present formalism which are given as

$$m_{S_2}, \sin\gamma, \kappa_{1i}, \kappa_{2i}, \kappa_{3i}, \kappa_{4i} \quad (i = 1, 2). \quad (44)$$

With the above choice of parameters the mixing between charged scalar particles (δ) becomes a dependent parameter. Masses of other scalars in dark sector S_1 , $S_{1,2}^\pm$ and $D^{\pm\pm}$ are also obtained using these free parameters. Moreover, we consider the case where the mixing between the neutral scalar particles satisfy the following condition $0 \leq \sin\gamma \leq \frac{1}{\sqrt{2}}$. For simplicity we also work with the following condition $\kappa_{11} = \kappa_{12}, \kappa_{21} = \kappa_{22}, \kappa_{31} = \kappa_{32}$ and $\kappa_{41} = \kappa_{42} (\neq 0)$. With the above mentioned choice of scalar mixing, we consider a parameter space depending on the choice of κ_{4i} and κ_{2i} ($i = 1, 2$) in order to obtain a viable DM candidate in our model. We tabulate how the choice of couplings determines whether DM is neutral or charged as shown in Table 2. It is to be noted that our conclusion in Table 2 is independent of the choice of couplings κ_{1i} and

Table 2

Combination of coupling parameters considered in the present work for the choice $0 \leq \sin \gamma \leq \frac{1}{\sqrt{2}}$.

κ_{41}	κ_{42}	κ_{21}	κ_{22}	DM candidate
-	-	+	+	S_1
-	-	-	-	S_1
+	+	-	-	S_2
+	+	+	+	Lightest inert particle is charged

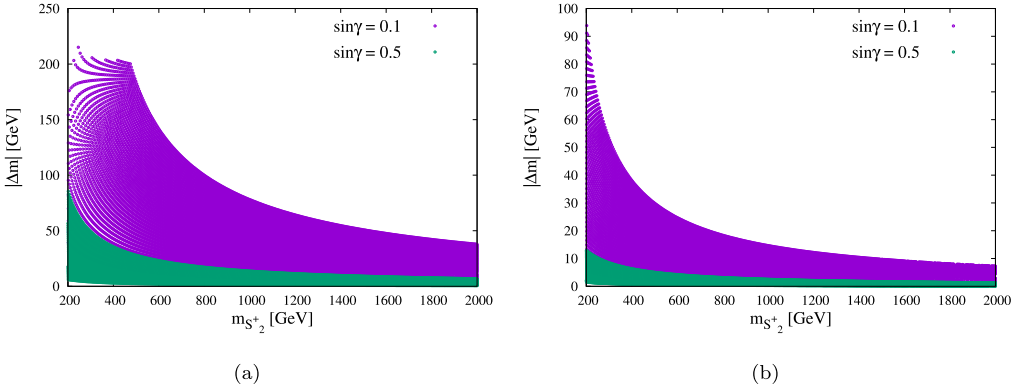


Fig. 3. Allowed range of mass splitting plotted against $m_{S_2^+}$ for different values of neutral scalar mixing angles with $\tan \beta = 1$ (left panel) and $\tan \beta = 10$ (right panel).

κ_{3i} ($i = 1, 2$). Therefore, in the present work, we consider only six relevant parameters to explore DM phenomenology, are given as

$$m_{S_2}, \sin \gamma, \kappa_{2i}, \kappa_{4i} \quad (i = 1, 2). \tag{45}$$

As observed in Table 2, we exclude the case with $\kappa_{21,22} > 0$ and $\kappa_{41,42} > 0$ values. Therefore, we are left with two cases, I) neutral DM candidate is represented by S_1 and II) DM is represented by S_2 . We will discuss both the cases separately in details in this section.

Before we discuss the DM phenomenology, we first consider the model parameter space in agreement with T parameter results. We consider a set of parameters following Table 2, a) $\kappa_{1i} = \kappa_{2i} = \kappa_{3i} = 0.05$ with κ_{4i} varying in the range of $[-0.5, -0.05]$ and b) $\kappa_{1i} = -\kappa_{2i} = \kappa_{3i} = 0.05$ with κ_{4i} varying in $[0.05, 0.5]$ ($i = 1, 2$). The above choice of parameters corresponds to first (third) row of Table 2 resulting S_1 (S_2) as the DM candidate. Since T parameter depends on the mass splitting, we observe that it is independent of the choice of sign of couplings mentioned in Table 2 and thus we ignore the second row of Table 2. We further consider two different values of neutral scalar mixing angle $\sin \gamma = 0.1, 0.5$ and vary mass m_{S_2} within the range 200 GeV to 2 TeV. With the above choice of parameters, one can easily derive masses of other dark sector particles and also the mixing angle δ between charged particles. Using the bound on T parameter, in Fig. 3(a) we plot the allowed range of mass splitting $|\Delta m| = |m_{S_2^+} - m_{S_1^+}|$ against $m_{S_2^+}$ derived following Eq. (36) for $\tan \beta = 1$. From Fig. 3(a), it can be easily stated that, larger values of mass splitting are allowed for smaller values of mixing angle. It is to be noted that for small mixing $\sin \gamma = 0.1$, triplet scalars are almost decoupled from each other which allows larger mass splitting values compared to the case with larger mixing $\sin \gamma = 0.5$. One can also

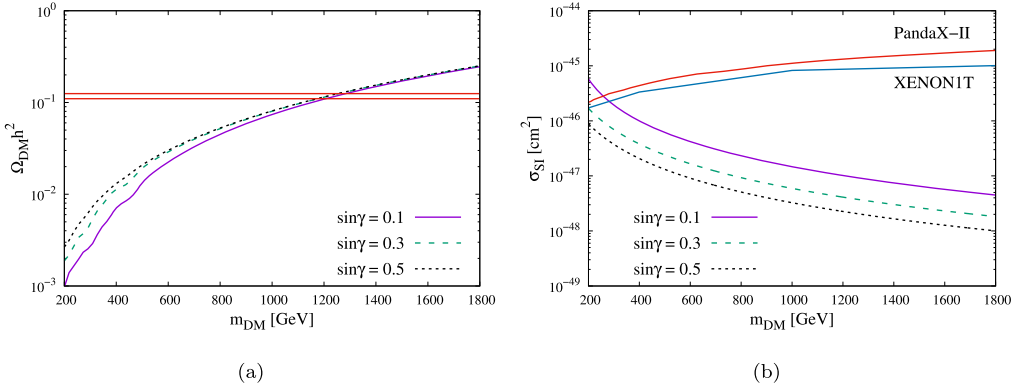


Fig. 4. Left panel: Variation of DM mass with relic abundance for different values of mixing angle γ (see text for details). Right panel: DM mass plotted against direct detection cross-section for the same set of parameters. (For interpretation of the colors in the figure(s), the reader is referred to the web version of this article.)

notice that as the mass $m_{S_2^+}$ is increased, mass difference of charged particles reduces and tends to become degenerate. Decrease in mass splitting enhances the possibility of co-annihilation of dark matter particles which can contribute to dark matter relic abundance. In, Fig. 3(b), we calculate the allowed range of parameter space for the same set of mixing angles $\sin \gamma$ and couplings for $\tan \beta = 10$. We observe that larger values of $\tan \beta$ constraints the model parameter space significantly allowing lesser values of mass splitting in agreement with the bound on T parameter. This is intriguing because of the fact that mass splitting between particles depends on both v_1 and v_2 vacuum expectation values.

3.4. Case: I, S_1 dark matter

In this section we study DM phenomenology for the case when DM is represented by S_1 candidate and resembles the T^0 candidate of $Y = 0$ triplet. We work with the conditions set by Table 2 for this purpose.

- Effects of $\sin \gamma$

In Fig. 4(a), we show the variation of DM relic density with mass of DM for three different values of $\sin \gamma = (0.1, 0.3, 0.5)$. Fig. 4(a) is plotted for $\tan \beta = 1$, $\kappa_{1i} = \kappa_{2i} = \kappa_{3i} = 0.05$ and $\kappa_{4i} = -0.05$ where $i = 1, 2$. In Fig. 4(b) the variation of dark matter direct detection against DM mass is depicted for same set of parameters and compares with the experimental bounds on DM-nucleon scattering cross-section with PandaX-II and XENON1T. It can be observed that changes in the mixing angle $\sin \gamma$ does not affect DM relic density very much and a 1.2 TeV dark matter candidate is in agreement with the relic density bound from PLANCK (red horizontal lines in left panel of Fig. 4). However, with increase in the mixing angle, the DM direct detection cross-section tends to decreases considerably. Therefore, large mixing angle $\sin \gamma$ is favorable for a viable DM candidate in the present framework.

- Effects of $\tan \beta$

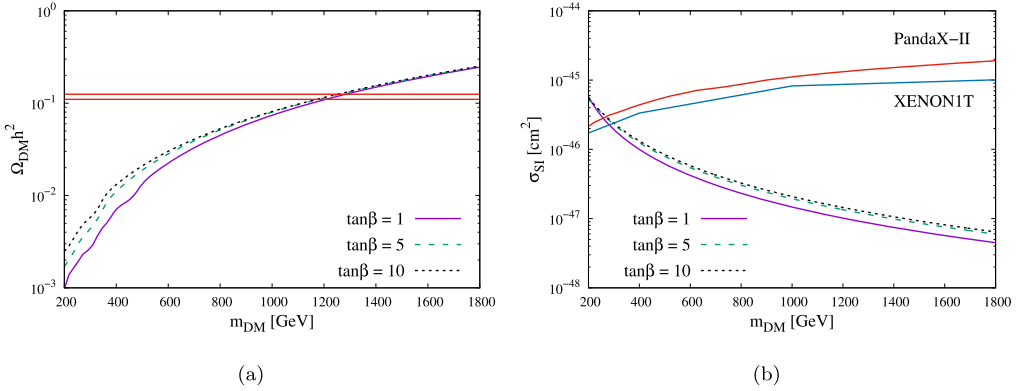


Fig. 5. Left panel: DM mass vs relic density for different $\tan\beta$. Right panel: DM mass vs direct detection cross-section plotted with same set of $\tan\beta$ values. See text for details.

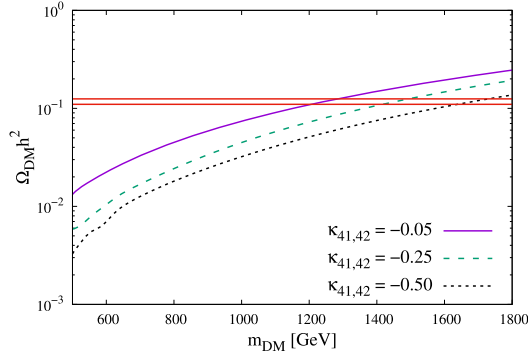


Fig. 6. Variation of DM relic abundance with DM mass for different values of $\kappa_{41,42}$ using $\sin\gamma = 0.1$ and $\tan\beta = 1$.

In Fig. 5, we repeat the results for dark matter with same set of coupling parameters as used in case of Fig. 4 for different values of $\tan\beta = (1, 5, 10)$ with scalar mixing fixed at $\sin\gamma = 0.1$. We observe in Fig. 5(a) that for different values of $\tan\beta$, DM relic abundance does not change significantly with DM mass. However, DM-nucleon scattering cross-section increases with larger $\tan\beta$ values as seen in Fig. 5(b).

- Effects of $\kappa_{41,42}$

Fig. 6 shows the variation of DM relic density against DM mass for three different values of $\kappa_{41,42}$ for $\tan\beta = 1$ and $\sin\gamma = 0.1$. Other parameter are kept fixed at same values as considered in Fig. 4. In Fig. 6 we observe that as $\kappa_{41,42}$ changes from -0.05 to -0.5 , relic density plots changes significantly which allows a range of dark matter mass from 1.2 TeV to 1.7 TeV that is in agreement with PLANCK results. Increase in $|\kappa_{41,42}|$ value results in increase in mass splitting between charged and neutral eigenstates $S_{1,2}^+$ and $S_{1,2}$. With increased mass splitting, contribution from co-annihilation channels decreases which reduces DM relic density for a given mass of DM as observed in Fig. 6. However, no significant change in DM direct detection is observed for changes in coupling $\kappa_{41,42}$.

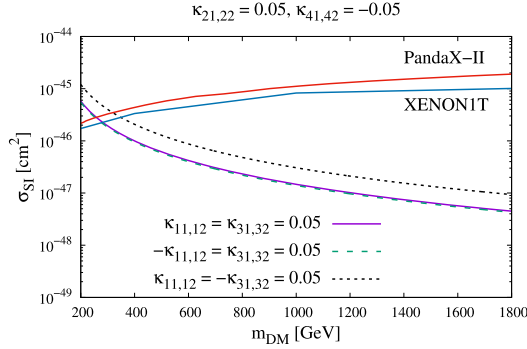


Fig. 7. DM mass vs σ_{SI} plots for different combinations of $\kappa_{11,12}$ and $\kappa_{31,32}$ using $\sin \gamma = 0.1$ and $\tan \beta = 1$.

- Effects of $\kappa_{11,12}$ and $\kappa_{31,32}$

Finally, we consider changes of couplings κ_{1i} and κ_{3i} , $i = 1, 2$ and study how these couplings affect dark matter phenomenology. It is found from the study that couplings κ_{1i} and κ_{3i} does not alter DM relic density significantly but can affect the DM direct detection cross-sections. This is obvious since, these couplings allow Higgs portal interactions with SM sector particles. However, since gauge interactions and co-annihilation channels dominate over Higgs portal interactions, these couplings are less sensitive to DM relic density. For the purpose of demonstration, we consider $\tan \beta = 1$, $\sin \gamma = 0.1$ and couplings $\kappa_{21,22}$, $\kappa_{41,42}$ etc. used in previous set of plots shown in Fig. 4–5. From Fig. 7, we observe that changing value of $\kappa_{11,12} = -0.05$ from $\kappa_{11,12} = 0.05$, does not affect direct detection results significantly. However, for the case $\kappa_{31,32} = -0.05$ an increase in DM direct detection is observed when compared with the case $\kappa_{31,32} = 0.05$. Therefore, we can conclude that $\kappa_{31,32} < 0$ enhances DM-nucleon scattering cross-section in the present framework.

It is to be noted that for DM candidate (S_1) there exists another region of parameter space with positive values of $\kappa_{21,22}$ as mentioned earlier in Table 2. We have found that the results for the region with positive $\kappa_{21,22}$ also follow similar behaviour as obtained in Figs. 4–8. Hence, DM phenomenology for the case with $\kappa_{21,22} > 0$ are not shown in this work.

3.5. Case: II, S_2 dark matter

In the previous section, we have presented the results for DM dominated by S_1 . In this section we consider the case when DM is S_2 dominated which resemble the neutral candidate of $Y = 1$ triplet. For this purpose, we follow the conditions mentioned in Table 2.

- Effects of $\sin \gamma$

Similar to the previous section, we now repeat our study for the case considering DM candidate is S_2 with positive values of $\kappa_{41,42}$ following Table 2. In Fig. 8(a)-(b), we show the variation of DM relic density and direct detection cross-section against DM mass for three different values of $\sin \gamma$ plotted with set of coupling parameters $\kappa_{11,12} = \kappa_{31,32} = \kappa_{41,42} = 0.05$ and $\kappa_{21,22} = -0.05$ using $\tan \beta = 1$. We observe that, even DM candidate is S_2 -like, with differ-

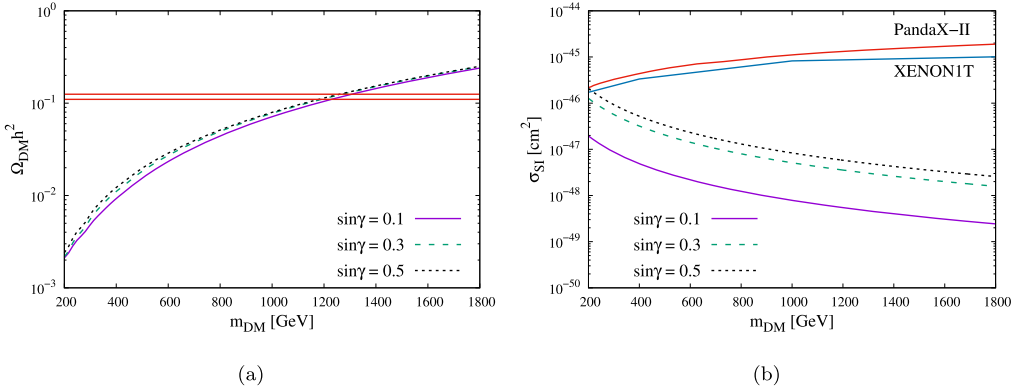


Fig. 8. Left panel: Variation of DM mass with relic abundance for different $\sin\gamma$. See text for details. Right panel: DM mass plotted against σ_{SI} for the same set of parameters.

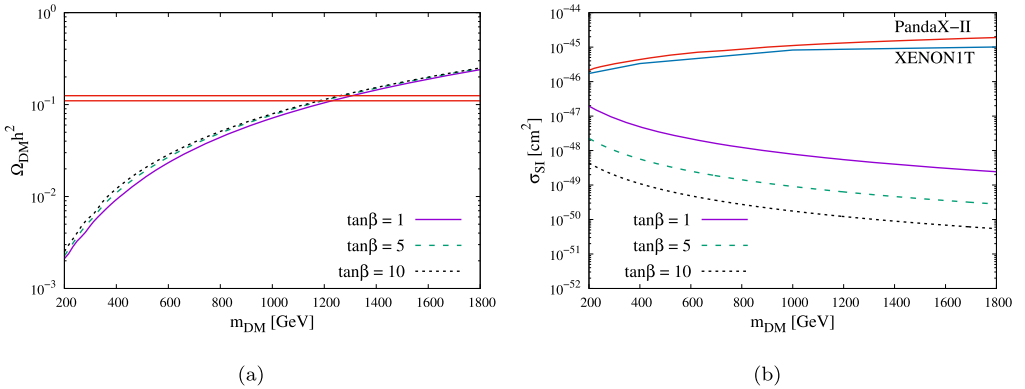


Fig. 9. Left panel: Dark matter mass vs relic density for different values of $\tan\beta$. See text for details. Right panel: DM mass against DM nucleon scattering cross-section for same set of $\tan\beta$ and other parameters.

ent $\sin\gamma$ values, DM mass versus relic density plots does not undergo any significant changes and 1.2 TeV dark matter satisfies DM relic density. However, significant changes in DM mass versus DM-nucleon scattering cross-section plot can be observed with changes in $\sin\gamma$ values as depicted in Fig. 8(b). It is clearly shown that with increasing $\sin\gamma$, the DM direct detection cross-section gains large enhancement. This is quite different when compared with the case of S_1 DM case presented in Fig. 4(b).

- Effects of $\tan\beta$

We now repeat the study with three different $\tan\beta = 1, 5, 10$ values for $\sin\gamma = 0.1$, keeping other parameters fixed as taken in previous case (Fig. 8), and present our findings in Fig. 9. From Fig. 9(a), we conclude that changes in $\tan\beta$ is less significant to DM relic density. However, Fig. 9(b) predicts that for larger $\tan\beta$, DM-nucleon cross-section tends to decrease.

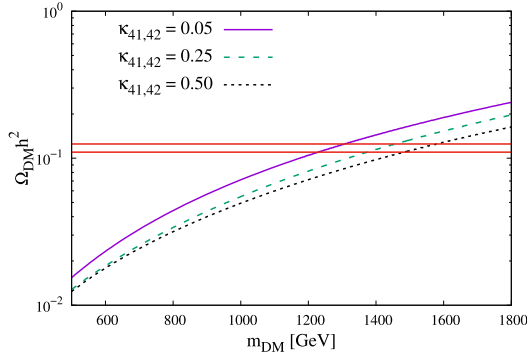


Fig. 10. DM mass vs relic density plots for different values of $\kappa_{41,42}$ using $\sin \gamma = 0.1$ and $\tan \beta = 1$.

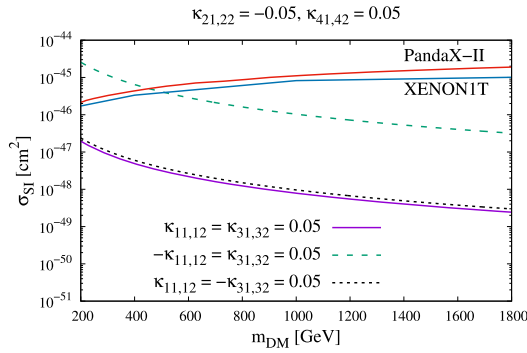


Fig. 11. Variation of DM mass with σ_{S1} for different choices of $\kappa_{11,12}$ and $\kappa_{31,32}$ using $\sin \gamma = 0.1$ and $\tan \beta = 1$.

- Effects of $\kappa_{41,42}$

In Fig. 10, we repeat our study following Fig. 6 by varying $\kappa_{41,42}$ from 0.05 to 0.5 for $\sin \gamma = 0.1$ and $\tan \beta = 1$ keeping the rest of the parameters unchanged as considered in Fig. 8. Similar to the case of dark matter in Fig. 6, here we also observe large changes in DM relic density which predicts that DM can have mass around 1.2 TeV to 1.6 TeV. This can be explained by the rise in mass splitting between dark sector particles which causes reduction in DM annihilation cross-section happening from DM co-annihilation. Note that, for different values of κ_{4i} ($i = 1 - 2$), DM direct detection cross-section remains unchanged similar to the case of S_1 dark matter.

- Effects of $\kappa_{11,12}$ and $\kappa_{31,32}$

Similar to the study of S_1 dark matter phenomenology performed in Fig. 7, we investigate the effects of $\kappa_{11,12}$ and $\kappa_{31,32}$ in Fig. 11 on DM-nucleon scattering cross-section. As we have mentioned before, due to the effects of gauge annihilations and co-annihilation of dark matter candidate, these couplings are not significant to DM relic abundance. Looking into Fig. 11, we conclude that dark matter direct detection results remains almost unaffected with change in sign of $\kappa_{31,32}$ from positive to negative. However, for the case $\kappa_{11,12} = -0.05$, there is significant enhancement in DM direct detection cross-section when compared with the case $\kappa_{11,12} = 0.05$,

Table 3

Combination of different coupling parameters for the choice $-\frac{1}{\sqrt{2}} \leq \sin \gamma \leq 0$.

κ_{41}	κ_{42}	κ_{21}	κ_{22}	DM candidate
+	+	+	+	S_1
+	+	-	-	S_1
-	-	-	-	S_2
-	-	+	+	Lightest inert particle is charged

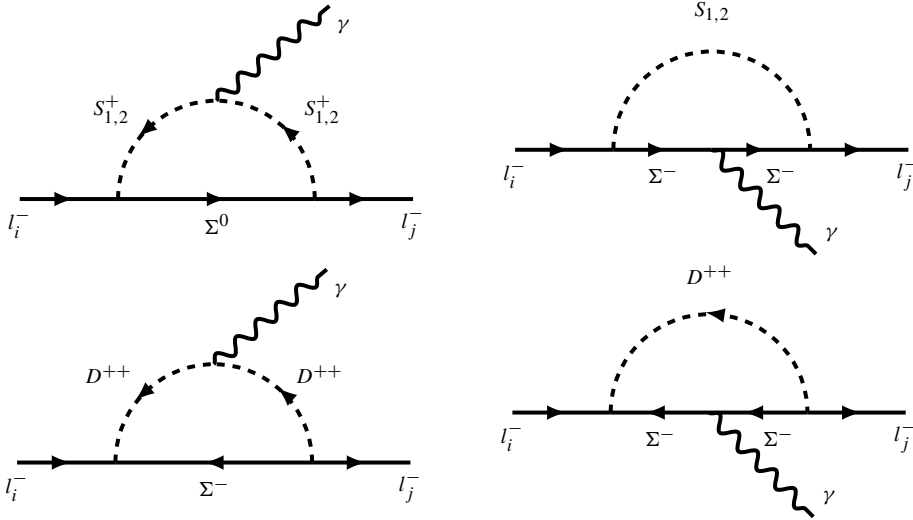


Fig. 12. $l_i \rightarrow l_j \gamma$ diagrams at the one-loop level.

which can be probed by next generation DM direct search experiments and constrain the available model parameter space.

It is to be noted that apart from the region of parameter space considered in Table 2, there also exists another region of available parameter space as given in Table 3 for $-\frac{1}{\sqrt{2}} \leq \sin \gamma \leq 0$. However, the DM phenomenology does not alter significantly for negative values of neutral scalar mixing $\sin \gamma$ and results are similar to cases discussed in Figs. 4–10. Therefore, we will not discuss the combination of parameter space mentioned in Table 3.

Therefore, DM phenomenology of 2HDM extension of inert GM model suggests that a viable TeV scale dark matter can be achieved within the framework. Since the masses of dark sector particles are around few TeVs, their contribution to the process $h \rightarrow \gamma \gamma$ is negligible compared to the contribution from W^\pm , H^\pm and fermion (top and bottom quarks) and thus can be ignored safely. In other words, conditions described in Eq. (43) for type-I 2HDM remains unaltered.

3.6. Lepton flavor violation

In the present model, Yukawa interactions mentioned in the Eq. (7) will result in charged lepton flavor violation. In Fig. 12, we show possible diagrams that contribute to flavor violating decay. The Feynman amplitude for the process $l_i \rightarrow l_j \gamma$ is given as

$$\mathcal{M}(l_i \rightarrow l_j \gamma) = \epsilon^\mu \bar{u}_{l_j}(p - q)[i q^\nu \sigma_{\mu\nu}(F + G\gamma_5)]u_{l_i}(p). \tag{46}$$

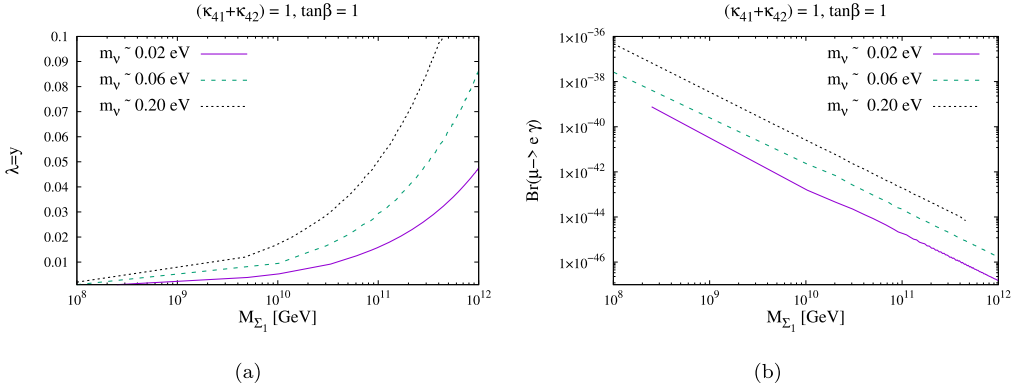


Fig. 13. Left panel: Variation of M_{Σ_1} with Yukawa coupling λ consistent with active neutrino mass constraints assuming $\lambda = y$ for $\tan\beta = 1$ and $|\kappa_{41,42}| = 0.5$. Right panel: Decay branching ratio $\mathcal{B}(\mu \rightarrow e\gamma)$ versus M_{Σ_1} for the allowed range of $\lambda = y$ coupling in agreement with limit from neutrino mass.

where the form factors F and G are expressed as

$$\begin{aligned}
 F = G = & \sum_{k=1}^3 \frac{\lambda_{ik}\lambda_{jk}}{64\pi^2 M_{\Sigma_k}^2} (m_{l_i} + m_{l_j})^2 \\
 & \times \left(\cos^2 \delta F_3^{(a)} + \sin^2 \delta F_4^{(a)} - \frac{1}{2} \cos^2 \gamma F_1^{(b)} - \frac{1}{2} \sin^2 \gamma F_2^{(b)} \right) \\
 & + \sum_{k=1}^3 \frac{y_{ik}y_{jk}}{64\pi^2 M_{\Sigma_k}^2} (m_{l_i} + m_{l_j})^2 \left(\sin^2 \delta F_3^{(a)} + \cos^2 \delta F_4^{(a)} + F_5^{(a)} - 2F_5^{(b)} \right) \\
 & + \sum_{k=1}^3 \frac{\lambda_{ik}y_{jk} + \lambda_{jk}y_{ik}}{64\pi^2 M_{\Sigma_k}^2} (m_{l_i} + m_{l_j})^2 \sin \delta \cos \delta \left(F_4^{(a)} - F_3^{(a)} \right),
 \end{aligned} \tag{47}$$

where,

$$\begin{aligned}
 F_i^{(a)} &= \frac{1}{6(1-x_i)^4} \left(2 + 3x_i - 6x_i^2 + x_i^3 + 6x_i \ln x_i \right), \\
 F_i^{(b)} &= \frac{1}{6(1-x_i)^4} \left(1 - 6x_i - 3x_i^2 - 2x_i^3 - 6x_i^2 \ln x_i \right), \\
 x_1 &= \frac{m_{S_1}^2}{M_{\Sigma}^2}, \quad x_2 = \frac{m_{S_2}^2}{M_{\Sigma}^2}, \quad x_3 = \frac{m_{S_1^+}^2}{M_{\Sigma}^2}, \quad x_4 = \frac{m_{S_2^+}^2}{M_{\Sigma}^2}, \quad x_5 = \frac{m_{D^{++}}^2}{M_{\Sigma}^2}.
 \end{aligned} \tag{48}$$

In Eq. (48), we have dropped the indices of M_{Σ_k} for simplicity. It is to be noted that for a vector fermion doublet $M_{\Sigma_k^0} = M_{\Sigma_k^+} = M_{\Sigma_k}$. Stringent bound on flavor violating process $\mu \rightarrow e\gamma$ is obtained from MEG experiment [67]. Upper limit on the decay branching ratio for $\mu \rightarrow e\gamma$ decay is $\mathcal{B}(\mu \rightarrow e\gamma) < 4.2 \times 10^{-13}$. The decay rate for the process $\mu \rightarrow e\gamma$ in the present model is given by

$$\Gamma(\mu \rightarrow e\gamma) = \frac{m_{\mu}}{8\pi} (|F|^2 + |G|^2). \tag{49}$$

In Fig. 13(a), we present the variation of vector fermion mass M_{Σ_1} with Yukawa couplings imposing the condition $\lambda = y$ for neutrino Yukawa couplings. The mass scale of light active neutrino mass (m_ν) is derived using Eq. (29) for $\tan\beta = 1$ and $|\kappa_{41,42}| = 0.5$ with assuming a hierarchical structure of vector fermion mass $M_{\Sigma_1} : M_{\Sigma_2} : M_{\Sigma_3} = 1 : 3 : 30$. We further consider mass of different inert scalar $m_S \sim 1.5$ TeV, following results from Fig. 6 and Fig. 10, consistent with relic density, direct detection, T parameter and collider constraints on dark matter. From Fig. 13(a), we notice that for Yukawa coupling ranging from $10^{-3} - 10^{-1}$, mass of vector fermion varies within the range $10^8 - 10^{12}$ GeV. Using the allowed range of M_{Σ_1} and Yukawa coupling values, we plot the corresponding decay branching ratio $\mathcal{B}(\mu \rightarrow e\gamma)$ against M_{Σ_1} , as shown in Fig. 13(b). It is clearly observed that within the specific range of $\lambda(y) - M_{\Sigma_1}$, $\mu \rightarrow e\gamma$ decay branching ratio is negligible compared to the experimental limit $\mathcal{B}(\mu \rightarrow e\gamma) < 4.2 \times 10^{-13}$ [67]. Therefore, lepton flavor violation do not impose any stringent limit in the present framework.

4. Leptogenesis in sGM model

Apart from the generation of one-loop neutrino mass and providing a feasible candidate for dark matter, the scotogenic GM model can also generate lepton asymmetry which can explain baryon asymmetry in the Universe (BAU). In the present model, heavy vector-like fermions can decay into leptons and triplets. A net asymmetry in lepton number can be generated from the CP violating decay of heavy vector-like fermions.

The net amount of asymmetry generated from CP violating decay of VLF's coming from its decay into leptons with two different scalar triplets are expressed as

$$\epsilon_{1\Delta} = \frac{\sum_\alpha [\Gamma(\Sigma \rightarrow l_L^c + \Delta) - \Gamma(\Sigma^c \rightarrow l_L + \Delta^*)]}{\Gamma_1}, \tag{50}$$

and

$$\epsilon_{1T} = \frac{\sum_\alpha [\Gamma(\Sigma^c \rightarrow l_L^c + T^*) - \Gamma(\Sigma \rightarrow l_L + T)]}{\Gamma_1}. \tag{51}$$

In the above Eq. (50)-(51), total decay width of vector fermion is given as

$$\Gamma_1 = \frac{3}{32\pi} \left((y^\dagger y)_{11} + (\lambda^\dagger \lambda)_{11} \right) M_{\Sigma_1}. \tag{52}$$

The asymmetry $\epsilon_{1\Delta}$ can be redefined as

$$\epsilon_{1\Delta} = -\frac{3}{8\pi} \frac{1}{(y^\dagger y)_{11} + (\lambda^\dagger \lambda)_{11}} \sum_j \text{Im}[(y^\dagger y)_{1j} (\lambda^T \lambda^*)_{j1}] \frac{M_{\Sigma_1}}{M_{\Sigma_j}}. \tag{53}$$

Similarly, the asymmetry ϵ_{1T} becomes

$$\epsilon_{1T} = -\frac{3}{8\pi} \frac{1}{(y^\dagger y)_{11} + (\lambda^\dagger \lambda)_{11}} \sum_j \text{Im}[(\lambda^\dagger \lambda)_{1j} (y^T y^*)_{j1}] \frac{M_{\Sigma_1}}{M_{\Sigma_j}}. \tag{54}$$

As mentioned before, in the following study we consider the mass matrix of vector-like fermions to be diagonal and assume hierarchical structure of vector-like fermion masses such that $M_{\Sigma_1} < M_{\Sigma_2} < M_{\Sigma_3}$ and $M_{\Sigma_1} : M_{\Sigma_2} : M_{\Sigma_3} = 1 : 3 : 30$. Therefore, Boltzmann equations for leptogenesis consist of three equations (which is governed by decay of lightest vector fermion)

$$\frac{dY_{\Sigma_1}}{dz} = -z \frac{\Gamma_1}{H_1} \frac{K_1(z)}{K_2(z)} \left(Y_{\Sigma_1} - Y_{\Sigma_1}^{\text{eq}} \right), \quad (55)$$

$$\frac{dY_L^\Delta}{dz} = -\frac{\Gamma_1}{H_1} \left(\epsilon_{1\Delta} z \frac{K_1(z)}{K_2(z)} (Y_{\Sigma_1}^{\text{eq}} - Y_{\Sigma_1}) + Br_L^\Delta \frac{z^3 K_1(z)}{4} Y_L^\Delta \right), \quad (56)$$

and

$$\frac{dY_L^T}{dz} = -\frac{\Gamma_1}{H_1} \left(\epsilon_{1T} z \frac{K_1(z)}{K_2(z)} (Y_{\Sigma_1}^{\text{eq}} - Y_{\Sigma_1}) + Br_L^T \frac{z^3 K_1(z)}{4} Y_L^T \right), \quad (57)$$

where Eq. (55) denotes Boltzmann equation for decay of vector-like fermion Σ_1 , other two Eqs. (56)-(57) are Boltzmann equations for generation of lepton asymmetry. In Eqs. (55)-(57), H_1 denotes the Hubble parameter at $T = M_{\Sigma_1}$ and $Y_x = n_x/s$; ($x = \Sigma_1, L, n$: number density and s : co-moving entropy density). The expression for H_1 and equilibrium yield of Σ_1 are

$$H_1 = \sqrt{\frac{8\pi G \rho_{\text{rad}}}{3}} = 1.66 \sqrt{g_*} \frac{M_{\Sigma_1}^2}{M_P}, \quad Y_{\Sigma_1}^{\text{eq}} = \frac{45g}{4\pi^4} \frac{z^2 K_2(z)}{g_{*s}}, \quad (58)$$

where $g_* = 119.75$ (including new scalar fields) is the relativistic degrees of freedom and g_{*s} is entropy degrees of freedom respectively. Factors $K_{1,2}$ in Eqs. (56)-(57) are modified Bessel functions and Br_L^x ($x = \Delta, T$) represent the decay branching fraction of Σ_1 into Δ and T mode such that

$$Br_L^\Delta = \frac{(y^\dagger y)_{11}}{(y^\dagger y)_{11} + (\lambda^\dagger \lambda)_{11}}, \quad Br_L^T = \frac{(\lambda^\dagger \lambda)_{11}}{(y^\dagger y)_{11} + (\lambda^\dagger \lambda)_{11}}. \quad (59)$$

It is to be noted that Boltzmann Eqs. (56)-(57) are based on the assumption that the transfer of asymmetry between Y_L^T and Y_L^Δ is negligible and their evolution are independent of each other. This is possible when the condition for the narrow width approximation is satisfied which is given as [68]

$$\frac{\Gamma_1}{H_1} \frac{\Gamma_1}{M_{\Sigma_1}} < 0.1. \quad (60)$$

The final lepton asymmetry obtained by solving Boltzmann equations for leptogenesis is given as

$$Y_L(z \rightarrow \infty) = 2 \left(Y_L^\Delta(z \rightarrow \infty) + Y_L^T(z \rightarrow \infty) \right). \quad (61)$$

In the above equation the additional factor of two is due to the fact that asymmetry is generated from both neutral and charged fermions of the vector fermion doublet. Eq. (61) reveals that, there can be a cancellation in net asymmetry $Y_L(z \rightarrow \infty)$. Similar to the case of standard leptogenesis with right handed neutrinos, here the final lepton asymmetry is also partially transferred into baryon asymmetry via sphaleron transition [17]

$$Y_B(z \rightarrow \infty) = \frac{10}{31} Y_L(z \rightarrow \infty). \quad (62)$$

Baryon asymmetry of the Universe as measured by PLANCK is $Y_B = (8 - 9.5) \times 10^{-11}$, hence the required lepton asymmetry is $Y_L \sim (2.5 - 2.9) \times 10^{-10}$ [2].

We now investigate the possibility whether the present model can generate the required BAU. In order to do so, we first consider Yukawa couplings and mass of vector-like fermions that will provide sub-eV light neutrino mass. For this purpose, we use the allowed M_{Σ_1} and Yukawa coupling $\lambda = y$ parameter space derived in Fig. 13(a) for neutrino mass scale $m_\nu = 0.02 - 0.20$

Table 4

Lepton asymmetry Y_L calculated using given set of vector fermion M_{Σ_1} mass and Yukawa coupling for $(\kappa_{41} + \kappa_{42}) = 1$, $\tan\beta = 1$ with different sets of Yukawa couplings $\{\lambda, y\}$ for neutrino mass scale $m_\nu \sim \mathcal{O}(10^{-2} - 10^{-1})$ eV.

Set	$\lambda = y$	M_{Σ_1} (GeV)	$\mathcal{O}(m_\nu)$ (eV)	$\epsilon_{1T,1\Delta}$	$Br_L^T = Br_L^\Delta$	$\frac{\Gamma_1}{H_1} \frac{\Gamma_1}{M_{\Sigma_1}}$	$Y_L(z \rightarrow \infty)$
I	4.0×10^{-2}	6.75×10^{11}	0.02	9.53×10^{-5}	0.5	8.1×10^{-2}	4.13×10^{-9}
II	2.1×10^{-2}	5.0×10^{10}	0.06	2.63×10^{-5}	0.5	8.3×10^{-2}	2.61×10^{-10}
III	1.1×10^{-2}	4.0×10^9	0.20	7.19×10^{-6}	0.5	7.8×10^{-2}	1.92×10^{-11}

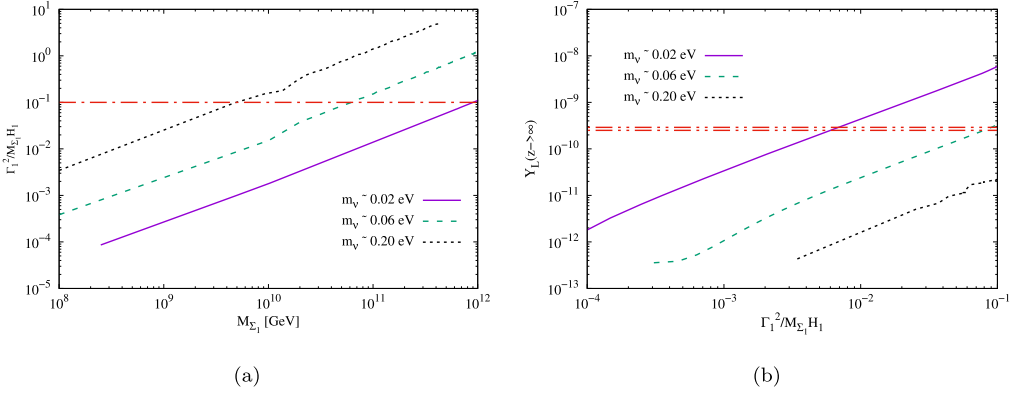


Fig. 14. Variation of M_{Σ_1} against $\Gamma_1^2/M_{\Sigma_1}H_1$ (left panel) and corresponding lepton asymmetry Y_L for $\Gamma_1^2/M_{\Sigma_1}H_1 < 0.1$ (right panel).

eV. Moreover, the Boltzmann equations for lepton asymmetry used are valid only when the condition for narrow width approximation in Eq. (60) is respected. It is found that the washout and transfer of asymmetry becomes significant for $\Gamma_1^2/M_{\Sigma_1}H_1 \geq 0.1$ [68]. To circumvent this issue, we further restrict the allowed M_{Σ_1} vs $\lambda = y$ parameter space in Fig. 13(a) with the condition $\Gamma_1^2/M_{\Sigma_1}H_1 < 0.1$. In Fig. 14(a), we present the variation of vector fermion mass M_{Σ_1} against the narrow width approximation parameter using the neutrino mass constraints from Fig. 13(a). The upper limit for narrow width approximation $\Gamma_1^2/M_{\Sigma_1}H_1 < 0.1$ is represented by the red horizontal line shown in Fig. 14(a). With the given range of neutrino mass scale $m_\nu = 0.02 - 0.20$ eV, Fig. 14(a) provides an upper limit on vector fermion mass for which narrow width approximation and the Boltzmann equations (Eqs. (56)-(57)) for lepton asymmetry remains valid.

Using the allowed range of M_{Σ_1} values obtained from Fig. 14(a) and Yukawa coupling from Fig. 13(a), we solve Boltzmann equations Eqs. (55)-(57) and evaluate the amount of lepton asymmetry in the present formalism. As to obtain the limits in Fig. 13(a) and Fig. 14(a), taking the condition $\lambda = y$ we get $\epsilon_{1\Delta} = \epsilon_{1T}$ and $Br_L^T = Br_L^\Delta = 1/2$. Therefore, for $\lambda = y$, lepton asymmetry generated from Eqs. (56)-(57) will be equal, i.e.; $Y_L^\Delta(z \rightarrow \infty) = Y_L^T(z \rightarrow \infty)$. In Fig. 14(b), we plot the total lepton asymmetry Y_L versus $\Gamma_1^2/M_{\Sigma_1}H_1$ using the available M_{Σ_1} parameter space obtained for aforementioned m_ν values. Horizontal red lines in Fig. 14(b) exhibit the Y_L value required to generate observed baryon asymmetry in the Universe. For demonstrative purpose, in Table 4, we tabulate lepton asymmetry Y_L for few sets of benchmark parameters obtained from the solutions of Boltzmann equations for leptogenesis. We observe that for benchmark set-I, yield of lepton asymmetry Y_L is above the required amount of matter-antimatter asymmetry. On

the other hand, for benchmark set-II with $m_\nu \sim 0.06$ eV, net lepton asymmetry Y_L successfully generates observed baryon abundance. However, set-III result in Table 4 suggests that yield Y_L fails to explain baryon asymmetry in the Universe.

It is worth mentioning that solution to Boltzmann equations in this work is based on the assumption that the Universe is radiation dominated at the era of leptogenesis. However, this situation can alter if one considers a modified thermal history of Universe [69]. Recent studies [70–73] reveal that non-standard cosmological effects (such as a new scalar field active near the temperature $T \sim M_{\Sigma_1}$) on leptogenesis can reduce the effects of washout significantly and enhance the yield of Y_L by one or two order depending on the new parameters. We expect similar changes in lepton asymmetry Y_L if non-standard cosmological effects are taken into account. In such scenarios, benchmark set-III of Table 4 can also explain matter-antimatter asymmetry in the Universe. Therefore, non-standard leptogenesis scenarios can relax constraints and broaden the available model parameter space considered in the model. However at lower temperature $T \sim 10^2 - 10^3$ TeV, the non-standard effect is completely washed out and Universe becomes radiation dominated. Therefore, thermal freeze-out of dark matter remains unaffected and hence dark matter phenomenology discussed in the work remains unharmed.

5. Conclusions

In this work we present a study of common origin of neutrino mass, dark matter and leptogenesis by extending Georgi-Machacek model with two Higgs doublet and new vector fermions. The composition of Georgi-Machacek model includes two additional $SU(2)$ triplet scalar with different hypercharge along with the SM Higgs doublet. Although the GM model preserves custodial symmetry and can generate neutrino mass in tree level, the model cannot account for a stable dark matter candidate. We consider a scalar potential invariant under $SU(2)_L \times U(1)_Y \times \mathcal{Z}_4 \times \mathcal{Z}_2$. After spontaneous breaking of symmetry, \mathcal{Z}_2 symmetry of the potential remains conserved by triplet fields and vector fermions. The \mathcal{Z}_4 symmetry in the potential provides necessary quartic interactions that generate neutrino mass at one-loop upon mixing of neutral and charged scalar of $Y = 0$ and $Y = 1$ triplet. Thus a residual \mathcal{Z}_2 symmetry ensures the stability of neutral scalar originating from the mixing of scalar triplets which serves the purpose of dark matter resulting a scotogenic Georgi-Machacek (sGM)model. Moreover, the sGM model also exhibits feature of leptogenesis, capable of generating matter-antimatter asymmetry in the Universe from decaying vector fermions.

We put constraints on the model parameter space from various theoretical and experimental observations, such as vacuum stability, dark matter relic abundance, dark matter direct detection cross-section. Detailed study of dark matter phenomenology reveals that the model predicts a TeV scale dark matter candidate. In the present model, matter-antimatter asymmetry originates from CP violating decay of vector-like fermions. Using the limits from light neutrino mass, we found that massive vector fermions around 10^{10-11} GeV can produce the experimentally observed baryon abundance. We have also observed that lepton flavor violation do not impose any significant constraint in the model parameter space. Therefore, a simple extension of Georgi-Machacek model with two Higgs doublet and heavy vector-like fermions accompanied by \mathcal{Z}_4 can provide answers to the puzzles of dark matter, matter-antimatter asymmetry in a single framework with radiative generation of neutrino mass.

CRedit authorship contribution statement

Shao-Long Chen: Conceptualization, Funding acquisition, Project administration, Supervision, Writing – review & editing. **Amit Dutta Banik:** Data curation, Formal analysis, Methodology, Software, Visualization, Writing – original draft, Writing – review & editing. **Ze-Kun Liu:** Data curation, Formal analysis, Software, Validation, Writing – review & editing.

Declaration of competing interest

The authors declare that they have no known competing financial interests or personal relationships that could have appeared to influence the work reported in this paper.

Acknowledgements

This work is supported in part by the National Science Foundation of China (11775093, 11422545, 11947235).

Appendix. SM Higgs coupling with charged scalars

The couplings of SM Higgs h with different charged scalars are listed as follows:

$$\begin{aligned}\lambda_{hD^{++}D^{--}} &= s_\alpha c_\beta \kappa_{11} - c_\alpha s_\beta \kappa_{12}, \\ \lambda_{hS_1^+ S_1^-} &= \frac{1}{2} (2s_\delta^2 s_\alpha c_\beta \kappa_{11} - 2s_\delta^2 c_\alpha s_\beta \kappa_{12} + s_\delta^2 s_\alpha c_\beta \kappa_{21} \\ &\quad - s_\delta^2 c_\alpha s_\beta \kappa_{22} + 2c_\delta^2 s_\alpha c_\beta \kappa_{31} - 2c_\delta^2 c_\alpha s_\beta \kappa_{32} - \sqrt{2} c_\delta s_\delta c_\alpha c_\beta \kappa_{41} \\ &\quad + \sqrt{2} c_\delta s_\delta s_\alpha s_\beta \kappa_{41} + \sqrt{2} c_\delta s_\delta s_\alpha s_\beta \kappa_{42} - \sqrt{2} c_\delta s_\delta c_\alpha c_\beta \kappa_{42}), \\ \lambda_{hS_2^+ S_2^-} &= \frac{1}{2} (2c_\delta^2 s_\alpha c_\beta \kappa_{11} - 2c_\delta^2 c_\alpha s_\beta \kappa_{12} + c_\delta^2 s_\alpha c_\beta \kappa_{21} - c_\delta^2 c_\alpha s_\beta \kappa_{22} \\ &\quad + 2s_\delta^2 s_\alpha c_\beta \kappa_{31} - 2s_\delta^2 c_\alpha s_\beta \kappa_{32} + \sqrt{2} c_\delta s_\delta c_\alpha c_\beta \kappa_{41} \\ &\quad - \sqrt{2} c_\delta s_\delta s_\alpha s_\beta \kappa_{41} - \sqrt{2} c_\delta s_\delta s_\alpha s_\beta \kappa_{42} + \sqrt{2} c_\delta s_\delta c_\alpha c_\beta \kappa_{42}), \\ \lambda_{hH^+ H^-} &= s_\alpha s_\beta^2 c_\beta \lambda_1 - c_\alpha c_\beta^2 s_\beta \lambda_2 - c_\alpha s_\beta^3 \lambda_3 + c_\beta^3 s_\alpha \lambda_3 \\ &\quad - c_\beta s_\alpha s_\beta^2 \lambda_4 + c_\alpha c_\beta^2 s_\beta \lambda_4 + c_\alpha c_\beta^2 s_\beta \lambda_5 - c_\beta s_\alpha s_\beta^2 \lambda_5.\end{aligned}$$

References

- [1] N. Aghanim, et al., Planck 2018 results. VI. Cosmological parameters, arXiv:1807.06209, 2018.
- [2] M. Tanabashi, et al., Particle Data Group, Review of particle physics, Phys. Rev. D 98 (2018) 030001, <https://doi.org/10.1103/PhysRevD.98.030001>.
- [3] P. Minkowski, $\mu \rightarrow e\gamma$ at a rate of one out of 10^9 muon decays?, Phys. Lett. B 67 (1977) 421–428, [https://doi.org/10.1016/0370-2693\(77\)90435-X](https://doi.org/10.1016/0370-2693(77)90435-X).
- [4] M. Gell-Mann, P. Ramond, R. Slansky, Complex spinors and unified theories, Conf. Proc. C 790927 (1979) 315–321, arXiv:1306.4669.
- [5] R.N. Mohapatra, G. Senjanovic, Neutrino mass and spontaneous parity nonconservation, Phys. Rev. Lett. 44 (1980) 912, <https://doi.org/10.1103/PhysRevLett.44.912>.
- [6] J. Schechter, J. Valle, Neutrino masses in $SU(2) \times U(1)$ theories, Phys. Rev. D 22 (1980) 2227, <https://doi.org/10.1103/PhysRevD.22.2227>.

- [7] R.N. Mohapatra, G. Senjanovic, Neutrino masses and mixings in gauge models with spontaneous parity violation, *Phys. Rev. D* 23 (1981) 165, <https://doi.org/10.1103/PhysRevD.23.165>.
- [8] C. Wetterich, Neutrino masses and the scale of B-L violation, *Nucl. Phys. B* 187 (1981) 343–375, [https://doi.org/10.1016/0550-3213\(81\)90279-0](https://doi.org/10.1016/0550-3213(81)90279-0).
- [9] J. Schechter, J. Valle, Neutrino decay and spontaneous violation of lepton number, *Phys. Rev. D* 25 (1982) 774, <https://doi.org/10.1103/PhysRevD.25.774>.
- [10] T. Hambye, G. Senjanovic, Consequences of triplet seesaw for leptogenesis, *Phys. Lett. B* 582 (2004) 73–81, <https://doi.org/10.1016/j.physletb.2003.11.061>, arXiv:hep-ph/0307237.
- [11] S. Antusch, Flavour-dependent type II leptogenesis, *Phys. Rev. D* 76 (2007) 023512, <https://doi.org/10.1103/PhysRevD.76.023512>, arXiv:0704.1591.
- [12] R. Foot, H. Lew, X. He, G.C. Joshi, Seesaw neutrino masses induced by a triplet of leptons, *Z. Phys. C* 44 (1989) 441, <https://doi.org/10.1007/BF01415558>.
- [13] S.-L. Chen, X.-G. He, Leptogenesis and LHC physics with type III see-saw, *Int. J. Mod. Phys. Conf. Ser.* 01 (2011) 18–27, <https://doi.org/10.1142/S2010194511000067>, arXiv:0901.1264.
- [14] M. Fukugita, T. Yanagida, Baryogenesis Without Grand Unification, *Phys. Lett. B* 174 (1986) 45–47, [https://doi.org/10.1016/0370-2693\(86\)91126-3](https://doi.org/10.1016/0370-2693(86)91126-3).
- [15] W. Buchmuller, P. Di Bari, M. Plumacher, Leptogenesis for pedestrians, *Ann. Phys.* 315 (2005) 305–351, <https://doi.org/10.1016/j.aop.2004.02.003>, arXiv:hep-ph/0401240.
- [16] W. Buchmuller, R. Peccei, T. Yanagida, Leptogenesis as the origin of matter, *Annu. Rev. Nucl. Part. Sci.* 55 (2005) 311–355, <https://doi.org/10.1146/annurev.nucl.55.090704.151558>, arXiv:hep-ph/0502169.
- [17] S. Davidson, E. Nardi, Y. Nir, Leptogenesis, *Phys. Rep.* 466 (2008) 105–177, <https://doi.org/10.1016/j.physrep.2008.06.002>, arXiv:0802.2962.
- [18] H. An, S.-L. Chen, R.N. Mohapatra, Y. Zhang, Leptogenesis as a common origin for matter and dark matter, *J. High Energy Phys.* 03 (2010) 124, [https://doi.org/10.1007/JHEP03\(2010\)124](https://doi.org/10.1007/JHEP03(2010)124), arXiv:0911.4463.
- [19] E. Ma, Verifiable radiative seesaw mechanism of neutrino mass and dark matter, *Phys. Rev. D* 73 (2006) 077301, <https://doi.org/10.1103/PhysRevD.73.077301>, arXiv:hep-ph/0601225.
- [20] S. Kashiwase, D. Suematsu, Baryon number asymmetry and dark matter in the neutrino mass model with an inert doublet, *Phys. Rev. D* 86 (2012) 053001, <https://doi.org/10.1103/PhysRevD.86.053001>, arXiv:1207.2594.
- [21] S. Kashiwase, D. Suematsu, Leptogenesis and dark matter detection in a TeV scale neutrino mass model with inverted mass hierarchy, *Eur. Phys. J. C* 73 (2013) 2484, <https://doi.org/10.1140/epjc/s10052-013-2484-9>, arXiv:1301.2087.
- [22] T. Hügler, M. Platscher, K. Schmitz, Low-scale leptogenesis in the scotogenic neutrino mass model, *Phys. Rev. D* 98 (2) (2018) 023020, <https://doi.org/10.1103/PhysRevD.98.023020>, arXiv:1804.09660.
- [23] W.-B. Lu, P.-H. Gu, Mixed inert scalar triplet dark matter, radiative neutrino masses and leptogenesis, *Nucl. Phys. B* 924 (2017) 279–311, <https://doi.org/10.1016/j.nuclphysb.2017.09.005>, arXiv:1611.02106.
- [24] Q.-H. Cao, S.-L. Chen, E. Ma, B. Yan, D.-M. Zhang, New class of two-loop neutrino mass models with distinguishable phenomenology, *Phys. Lett. B* 779 (2018) 430–435, <https://doi.org/10.1016/j.physletb.2018.02.038>, arXiv:1707.05896.
- [25] H. Zhou, P.-H. Gu, From high-scale leptogenesis to low-scale one-loop neutrino mass generation, *Nucl. Phys. B* 927 (2018) 184–195, <https://doi.org/10.1016/j.nuclphysb.2017.12.016>, arXiv:1708.04207.
- [26] P.-H. Gu, H.-J. He, TeV scale neutrino mass generation, minimal inelastic dark matter, and high scale leptogenesis, *Phys. Rev. D* 99 (1) (2019) 015025, <https://doi.org/10.1103/PhysRevD.99.015025>, arXiv:1808.09377.
- [27] A. Dutta Banik, R. Roshan, A. Sil, Neutrino mass and asymmetric dark matter: study with inert Higgs doublet and high scale validity (11 2020), arXiv:2011.04371.
- [28] R.A. Lineros, M. Pierre, Dark matter candidates in a type-II radiative neutrino mass model (11 2020), arXiv:2011.08195.
- [29] H. Haber, G. Kane, T. Sterling, The fermion mass scale and possible effects of Higgs bosons on experimental observables, *Nucl. Phys. B* 161 (2) (1979) 493–532, [https://doi.org/10.1016/0550-3213\(79\)90225-6](https://doi.org/10.1016/0550-3213(79)90225-6).
- [30] L.J. Hall, M.B. Wise, Flavor changing Higgs boson couplings, *Nucl. Phys. B* 187 (3) (1981) 397–408, [https://doi.org/10.1016/0550-3213\(81\)90469-7](https://doi.org/10.1016/0550-3213(81)90469-7).
- [31] V. Barger, J.L. Hewett, R.J.N. Phillips, New constraints on the charged Higgs sector in two-Higgs-doublet models, *Phys. Rev. D* 41 (1990) 3421–3441, <https://doi.org/10.1103/PhysRevD.41.3421>.
- [32] G.C. Branco, P.M. Ferreira, L. Lavoura, M.N. Rebelo, M. Sher, J.P. Silva, Theory and phenomenology of two-Higgs-doublet models, *Phys. Rep.* 516 (2012) 1–102, <https://doi.org/10.1016/j.physrep.2012.02.002>, arXiv:1106.0034.
- [33] H. Georgi, M. Machacek, Doubly charged Higgs bosons, *Nucl. Phys. B* 262 (1985) 463–477, [https://doi.org/10.1016/0550-3213\(85\)90325-6](https://doi.org/10.1016/0550-3213(85)90325-6).

- [34] M.S. Chanowitz, M. Golden, Higgs boson triplets with $M(W) = M(Z) \cos \theta \omega$, Phys. Lett. B 165 (1985) 105–108, [https://doi.org/10.1016/0370-2693\(85\)90700-2](https://doi.org/10.1016/0370-2693(85)90700-2).
- [35] J. Gunion, R. Vega, J. Wudka, Higgs triplets in the standard model, Phys. Rev. D 42 (1990) 1673–1691, <https://doi.org/10.1103/PhysRevD.42.1673>.
- [36] K. Hartling, K. Kumar, H.E. Logan, The decoupling limit in the Georgi-Machacek model, Phys. Rev. D 90 (1) (2014) 015007, <https://doi.org/10.1103/PhysRevD.90.015007>, arXiv:1404.2640.
- [37] C.-W. Chiang, K. Tsumura, Properties and searches of the exotic neutral Higgs bosons in the Georgi-Machacek model, J. High Energy Phys. 04 (2015) 113, [https://doi.org/10.1007/JHEP04\(2015\)113](https://doi.org/10.1007/JHEP04(2015)113), arXiv:1501.04257.
- [38] C.-W. Chiang, S. Kanemura, K. Yagyu, Phenomenology of the Georgi-Machacek model at future electron-positron colliders, Phys. Rev. D 93 (5) (2016) 055002, <https://doi.org/10.1103/PhysRevD.93.055002>, arXiv:1510.06297.
- [39] C.-W. Chiang, G. Cottin, O. Eberhardt, Global fits in the Georgi-Machacek model, Phys. Rev. D 99 (1) (2019) 015001, <https://doi.org/10.1103/PhysRevD.99.015001>, arXiv:1807.10660.
- [40] D. Das, I. Saha, Cornering variants of the Georgi-Machacek model using Higgs precision data, Phys. Rev. D 98 (9) (2018) 095010, <https://doi.org/10.1103/PhysRevD.98.095010>, arXiv:1811.00979.
- [41] J. Chakraborty, P. Konar, T. Mondal, Copositive criteria and boundedness of the scalar potential, Phys. Rev. D 89 (9) (2014) 095008, <https://doi.org/10.1103/PhysRevD.89.095008>, arXiv:1311.5666.
- [42] L. Ping, F.Y. Yu, Criteria for copositive matrices of order four, Linear Algebra Appl. 194 (1993) 109–124, [https://doi.org/10.1016/0024-3795\(93\)90116-6](https://doi.org/10.1016/0024-3795(93)90116-6).
- [43] J. Gunion, R. Vega, J. Wudka, Naturalness problems for $\rho = 1$ and other large one loop effects for a standard model Higgs sector containing triplet fields, Phys. Rev. D 43 (1991) 2322–2336, <https://doi.org/10.1103/PhysRevD.43.2322>.
- [44] S. Blasi, S. De Curtis, K. Yagyu, Effects of custodial symmetry breaking in the Georgi-Machacek model at high energies, Phys. Rev. D 96 (1) (2017) 015001, <https://doi.org/10.1103/PhysRevD.96.015001>, arXiv:1704.08512.
- [45] B. Keeshan, H.E. Logan, T. Pilkington, Custodial symmetry violation in the Georgi-Machacek model, Phys. Rev. D 102 (1) (2020) 015001, <https://doi.org/10.1103/PhysRevD.102.015001>, arXiv:1807.11511.
- [46] G. Cynolter, E. Lendvai, Electroweak precision constraints on vector-like fermions, Eur. Phys. J. C 58 (2008) 463–469, <https://doi.org/10.1140/epjc/s10052-008-0771-7>, arXiv:0804.4080.
- [47] H.-J. He, N. Polonsky, S.-f. Su, Extra families, Higgs spectrum and oblique corrections, Phys. Rev. D 64 (2001) 053004, <https://doi.org/10.1103/PhysRevD.64.053004>, arXiv:hep-ph/0102144.
- [48] W. Grimus, L. Lavoura, O.M. Ogreid, P. Osland, A precision constraint on multi-Higgs-doublet models, J. Phys. G 35 (2008) 075001, <https://doi.org/10.1088/0954-3899/35/7/075001>, arXiv:0711.4022.
- [49] W. Grimus, L. Lavoura, O.M. Ogreid, P. Osland, The oblique parameters in multi-Higgs-doublet models, Nucl. Phys. B 801 (2008) 81–96, <https://doi.org/10.1016/j.nuclphysb.2008.04.019>, arXiv:0802.4353.
- [50] G. Abbiendi, et al., Search for charged Higgs bosons: combined results using LEP data, Eur. Phys. J. C 73 (2013) 2463, <https://doi.org/10.1140/epjc/s10052-013-2463-1>, arXiv:1301.6065.
- [51] J. Abdallah, et al., Searches for supersymmetric particles in e^+e^- collisions up to 208-GeV and interpretation of the results within the MSSM, Eur. Phys. J. C 31 (2003) 421–479, <https://doi.org/10.1140/epjc/s2003-01355-5>, arXiv:hep-ex/0311019.
- [52] P. Achard, et al., Search for heavy neutral and charged leptons in e^+e^- annihilation at LEP, Phys. Lett. B 517 (2001) 75–85, [https://doi.org/10.1016/S0370-2693\(01\)01005-X](https://doi.org/10.1016/S0370-2693(01)01005-X), arXiv:hep-ex/0107015.
- [53] M. Aaboud, et al., Measurements of Higgs boson properties in the diphoton decay channel with 36 fb^{-1} of pp collision data at $\sqrt{s} = 13 \text{ TeV}$ with the ATLAS detector, Phys. Rev. D 98 (2018) 052005, <https://doi.org/10.1103/PhysRevD.98.052005>, arXiv:1802.04146.
- [54] A.M. Sirunyan, et al., Combined measurements of Higgs boson couplings in proton–proton collisions at $\sqrt{s} = 13 \text{ TeV}$, Eur. Phys. J. C 79 (5) (2019) 421, <https://doi.org/10.1140/epjc/s10052-019-6909-y>, arXiv:1809.10733.
- [55] G. Arcadi, 2HDM portal for singlet-doublet dark matter, Eur. Phys. J. C 78 (10) (2018) 864, <https://doi.org/10.1140/epjc/s10052-018-6327-6>, arXiv:1804.04930.
- [56] V. Khachatryan, et al., Precise determination of the mass of the Higgs boson and tests of compatibility of its couplings with the standard model predictions using proton collisions at 7 and 8 TeV, Eur. Phys. J. C 75 (5) (2015) 212, <https://doi.org/10.1140/epjc/s10052-015-3351-7>, arXiv:1412.8662.
- [57] G. Aad, et al., Measurements of the Higgs boson production and decay rates and coupling strengths using pp collision data at $\sqrt{s} = 7$ and 8 TeV in the ATLAS experiment, Eur. Phys. J. C 76 (1) (2016) 6, <https://doi.org/10.1140/epjc/s10052-015-3769-y>, arXiv:1507.04548.
- [58] M. Bauer, M. Klassen, V. Tenorth, Universal properties of pseudoscalar mediators in dark matter extensions of 2HDMs, J. High Energy Phys. 07 (2018) 107, [https://doi.org/10.1007/JHEP07\(2018\)107](https://doi.org/10.1007/JHEP07(2018)107), arXiv:1712.06597.
- [59] Y. Amhis, et al., Averages of b -hadron, c -hadron, and τ -lepton properties as of summer 2016, Eur. Phys. J. C 77 (12) (2017) 895, <https://doi.org/10.1140/epjc/s10052-017-5058-4>, arXiv:1612.07233.

- [60] A. Arbey, F. Mahmoudi, O. Stal, T. Stefaniak, Status of the charged Higgs boson in two Higgs doublet models, *Eur. Phys. J. C* 78 (3) (2018) 182, <https://doi.org/10.1140/epjc/s10052-018-5651-1>, arXiv:1706.07414.
- [61] A. Semenov, LanHEP: a package for the automatic generation of Feynman rules in field theory. Version 3.0, *Comput. Phys. Commun.* 180 (2009) 431–454, <https://doi.org/10.1016/j.cpc.2008.10.012>, arXiv:0805.0555.
- [62] G. Belanger, F. Boudjema, A. Pukhov, A. Semenov, MicrOMEGAs: a program for calculating the relic density in the MSSM, *Comput. Phys. Commun.* 149 (2002) 103–120, [https://doi.org/10.1016/S0010-4655\(02\)00596-9](https://doi.org/10.1016/S0010-4655(02)00596-9), arXiv:hep-ph/0112278.
- [63] E. Aprile, et al., Dark matter search results from a one tonne \times year exposure of XENON1T, arXiv:1805.12562, 2018.
- [64] E. Aprile, et al., Physics reach of the XENON1T dark matter experiment, *J. Cosmol. Astropart. Phys.* 1604 (04) (2016) 027, <https://doi.org/10.1088/1475-7516/2016/04/027>, arXiv:1512.07501.
- [65] A. Tan, et al., Dark matter results from first 98.7 days of data from the PandaX-II experiment, *Phys. Rev. Lett.* 117 (12) (2016) 121303, <https://doi.org/10.1103/PhysRevLett.117.121303>, arXiv:1607.07400.
- [66] X. Cui, et al., Dark matter results from 54-ton-day exposure of PandaX-II experiment, arXiv:1708.06917, 2017.
- [67] A. Baldini, et al., Search for the lepton flavour violating decay $\mu^+ \rightarrow e^+ \gamma$ with the full dataset of the MEG experiment, *Eur. Phys. J. C* 76 (8) (2016) 434, <https://doi.org/10.1140/epjc/s10052-016-4271-x>, arXiv:1605.05081.
- [68] A. Falkowski, J.T. Ruderman, T. Volansky, Asymmetric dark matter from leptogenesis, *J. High Energy Phys.* 05 (2011) 106, [https://doi.org/10.1007/JHEP05\(2011\)106](https://doi.org/10.1007/JHEP05(2011)106), arXiv:1101.4936.
- [69] F. D’Eramo, N. Fernandez, S. Profumo, When the universe expands too fast: relentless dark matter, *J. Cosmol. Astropart. Phys.* 05 (2017) 012, <https://doi.org/10.1088/1475-7516/2017/05/012>, arXiv:1703.04793.
- [70] B. Dutta, C.S. Fong, E. Jimenez, E. Nardi, A cosmological pathway to testable leptogenesis, *J. Cosmol. Astropart. Phys.* 10 (2018) 025, <https://doi.org/10.1088/1475-7516/2018/10/025>, arXiv:1804.07676.
- [71] S.-L. Chen, A. Dutta Banik, Z.-K. Liu, Leptogenesis in fast expanding universe, *J. Cosmol. Astropart. Phys.* 03 (2020) 009, <https://doi.org/10.1088/1475-7516/2020/03/009>, arXiv:1912.07185.
- [72] D. Mahanta, D. Borah, TeV scale leptogenesis with dark matter in non-standard cosmology, *J. Cosmol. Astropart. Phys.* 04 (04) (2020) 032, <https://doi.org/10.1088/1475-7516/2020/04/032>, arXiv:1912.09726.
- [73] P. Konar, A. Mukherjee, A.K. Saha, S. Show, A dark clue to seesaw and leptogenesis in singlet doublet scenario with (non)standard cosmology (7 2020), arXiv:2007.15608.